

**AD-A248 383**



PL-TR-91-2281

DTIC E200947  
ELECTE  
MAR 2 1992  
S c D

(2)

**ANALYSIS OF THE EFFECTS OF EURASIAN CRUSTAL  
AND UPPER MANTLE STRUCTURE ON REGIONAL PHASES  
USING BROADBAND SEISMIC DATA**

Susan Schwartz  
Thorne Lay

University of California, Santa Cruz  
Institute of Tectonics  
Santa Cruz, CA 95064

25 October 1991

Scientific Report No. 1

APPROVED FOR PUBLIC RELEASE; DISTRIBUTION UNLIMITED



PHILLIPS LABORATORY  
AIR FORCE SYSTEMS COMMAND  
HANSCom AIR FORCE BASE, MASSACHUSETTS 01731-5000

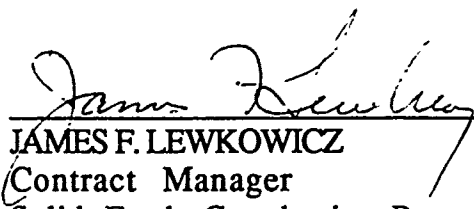
92 3 10 062

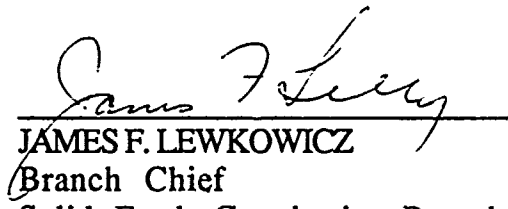
**92-06336**



The views and conclusions contained in this document are those of the authors and should not be interpreted as representing the official policies, either expressed or implied, of the Air Force or the U.S. Government.

This technical report has been reviewed and is approved for publication.

  
JAMES F. LEWKOWICZ  
Contract Manager  
Solid Earth Geophysics Branch  
Earth Sciences Division

  
JAMES F. LEWKOWICZ  
Branch Chief  
Solid Earth Geophysics Branch  
Earth Sciences Division

  
DONALD H. ECKHARDT, Director  
Earth Sciences Division

This document has been reviewed by the ESD Public Affairs Office (PA) and is releasable to the National Technical Information Service (NTIS).

Qualified requestors may obtain additional copies from the Defense Technical Information Center. All others should apply to the National Technical Information Service.

If your address has changed, or if you wish to be removed from the mailing list, or if the addressee is no longer employed by your organization, please notify PL/IMA, Hanscom AFB MA 01731-5000. This will assist us in maintaining a current mailing list.

Do not return copies of this report unless contractual obligations or notices on a specific document requires that it be returned.

**REPORT DOCUMENTATION PAGE**Form Approved  
OMB No. 0704-0188

Public reporting burden for this collection of information is estimated to average 1 hour per response, including the time for reviewing instructions, searching existing data sources, gathering and maintaining the data needed, and completing and reviewing the collection of information. Send comments regarding this burden estimate or any other aspect of this collection of information, including suggestions for reducing this burden, to Washington Headquarters Services, Directorate for Information Operations and Reports, 1215 Jefferson Davis Highway, Suite 1204, Arlington, VA 22202-4302, and to the Office of Management and Budget, Paperwork Reduction Project (0704-0188), Washington, DC 20503.

<b>1. AGENCY USE ONLY (Leave blank)</b>		<b>2. REPORT DATE</b> October 25, 1991	<b>3. REPORT TYPE AND DATES COVERED</b> Scientific Report #1	
<b>4. TITLE AND SUBTITLE</b> Analysis of the effects of Eurasian crustal and upper mantle structure on regional phases using broadband seismic data			<b>5. FUNDING NUMBERS</b> PE62101F PR7600 TA09 WUAP Contract F19628-90-K-0041	
<b>6. AUTHOR(S)</b> Susan Schwartz and Thorne Lay				
<b>7. PERFORMING ORGANIZATION NAME(S) AND ADDRESS(ES)</b> Institute of Tectonics University of California, Santa Cruz Santa Cruz, CA 95064			<b>8. PERFORMING ORGANIZATION REPORT NUMBER</b>	
<b>9. SPONSORING/MONITORING AGENCY NAME(S) AND ADDRESS(ES)</b> Phillips Laboratory Hanscom AFB, MA 01731-5000  Contract Manager: James Lewkowicz/GPEH			<b>10. SPONSORING/MONITORING AGENCY REPORT NUMBER</b>  PL-TR-91-2281	
<b>11. SUPPLEMENTARY NOTES</b>				
<b>12a. DISTRIBUTION / AVAILABILITY STATEMENT</b> Approved for public release; Distribution unlimited			<b>12b. DISTRIBUTION CODE</b>	
<b>13. ABSTRACT (Maximum 200 words)</b> This report represents the results of the first phase of our two year investigation of the effects of upper mantle structure on the propagation of regional phases. Our first year of effort has been directed at improving our understanding of the PP phase observed at upper mantle distances, and developing a methodology by which this phase can be used to map out large-scale variations in uppermost mantle velocity gradients and absolute velocity levels. We have been quite successful in quantifying the complex wavefield associated with PP, and present a preliminary application of PP waveform analysis across the North American continent, where we have lots of independent knowledge of the structure with which to assess the resulting models. Our next effort will be directed at application of the new methodology to mapping lid structure variations in Eurasia, combined with assessment of how these lid variations influence regional phase propagation and the behavior of various discriminant procedures such as Pn/Lg spectral behavior.				
<b>14. SUBJECT TERMS</b> Upper Mantle Velocities Wave Propagation Whispering Galleries			<b>15. NUMBER OF PAGES</b> 46	
			<b>16. PRICE CODE</b>	
<b>17. SECURITY CLASSIFICATION OF REPORT</b> Unclassified	<b>18. SECURITY CLASSIFICATION OF THIS PAGE</b> Unclassified	<b>19. SECURITY CLASSIFICATION OF ABSTRACT</b> Unclassified	<b>20. LIMITATION OF ABSTRACT</b> SAR	

## Table of Contents:

1. Introduction	1
2. Synthetic PP Waveforms at Upper Mantle Distances	2
2.1 Whispering Gallery Modes	6
2.2 Crustal Reverberations	8
3. PP Observations and Waveform Modeling	10
3.1 Upper Mantle P Wave Velocity Models	11
4. Conclusions	14
5. References	17



Accession For	
NEIS GRA&I	<input checked="" type="checkbox"/>
DTIC TAB	<input type="checkbox"/>
Unannounced	<input type="checkbox"/>
Justification	
By _____	
Distribution/	
Availability Codes	
Dist	Avail and/or Special
A-1	

## SUMMARY

We analyze the PP phase at upper mantle distances ( $25^\circ$  to  $60^\circ$ ) to quantify its propagation characteristics and potential for determining crust and upper mantle velocity structure. Upper mantle distance PP waveforms are very complex, involving interference between a variety of arrivals traversing different depth ranges in the Earth. These arrivals include PP triplications produced by the two major (and any other) upper mantle seismic discontinuities; energy that turns in the upper mantle and reflects from the underside of the Moho (e.g.  $P_mP$ ); and multiply reflected or converted phases in the crust at the source, receiver and PP mid-path bounce point (PP coupled PL). Even for laterally homogeneous structures, complete synthetic seismograms such as provided by reflectivity calculations are required to adequately model the full suite of arrivals that contribute to upper mantle PP phases. The complexity of PP waveforms can be exploited to extract crust and upper mantle structural information for relatively homogeneous paths, but the numerous interfering phases make it difficult to attribute PP characteristics to particular structural features without some *a priori* information. PP-P differential travel times and PP/P amplitude ratios provide constraints on average upper mantle velocities above the transition zone if the general crustal properties along the path are known. Often *a priori* information on crustal thickness is available and average lid velocity structure can thus be determined. Large amplitude early PP coda, comprised of crustal reflections and conversions, can provide information on crustal thickness and must be accounted for when identifying secondary upper mantle PP triplication branches.

It is also possible to place some constraints on the velocity gradients in the uppermost mantle. In the presence of a positive velocity gradient below the crust, whispering gallery multiple underside reflections from the Moho can be observed at upper mantle distances. The amplitudes of these Moho whispering gallery arrivals and associated underside reflections ( $P_mP$ ,  $P_mP_mP$ , etc.) are sensitive to the lid velocity gradient, particularly for short-period and broadband data at distances from  $25^\circ$  to  $38^\circ$ . We demonstrate the potential of accurate PP waveform modeling for determining upper mantle structure by modeling long-period signals traversing relatively 'pure' paths across North America. A continuum of P wave velocity models with varying lid structure is appropriate for the upper mantle beneath North America. The highest velocities are found beneath the northern Canadian shield, with the lid becoming progressively lower velocity beneath the southern shield, continental platform and tectonically active regions respectively. Most of the heterogeneity in P velocity structure is concentrated above a depth of 250 km, although some data are consistent with models that are relatively slow at greater depths. Refinement of these models, and full exploitation of the PP phase will require extensive broadband data

sets and two- and three-dimensional synthetic capabilities that can handle the intrinsic complexity of PP in the presence of lateral heterogeneity.

## 1 INTRODUCTION

Calculation of synthetic seismograms has contributed significantly to our knowledge of the Earth's velocity structure by allowing waveforms from many diverse phases to be successfully modeled or inverted for deep structure. A variety of techniques are now available for the computation of theoretical body wave seismograms in realistic Earth models and the choice of method for a particular application is usually determined through a compromise between the desired accuracy and the time and expense required to perform the calculation. The WKBJ algorithm in its original form (Chapman 1978) is exceptionally fast but involves significant approximations, reducing its suitability for some applications. The Cagniard-de Hoop method (e.g., Helmberger 1973, 1983) has fewer limitations and provides superb insight into the seismogram construction, but like the WKBJ method it requires specification of the rayset to be considered. The reflectivity technique (Fuchs & Müller 1971) employs propagator matrices to account for all conversions and reflections in a stratified medium, and is thus quite accurate and complete, but the method is relatively costly and it is often difficult to gain insight into the nature of individual arrivals. These procedures have been extensively compared and their respective limitations are well understood in general (e.g., Burdick & Orcutt 1979; Chapman and Orcutt 1985). Many additional procedures and hybrid methods have been developed for application in both layered and laterally heterogeneous structures. Richards (1985) provides a review of many applications of synthetic seismogram modeling for determining structure of the crust, mantle, and core.

The principal phases used for characterizing upper mantle structure have been direct P and S phases that interact with the transition zone velocity discontinuities to produce upper mantle triplications, reflections and conversions. In order to expand the spatial coverage of upper mantle structure, seismologists have begun to model later phases, involving multiple surface and/or core reflections along their path. The application of WKBJ and Cagniard-de Hoop synthetic modeling to multiple bounce transverse shear waves (SS and SSS) was instrumental in establishing the magnitude and depth extent of lateral variations in the upper mantle shear wave velocity structure beneath North America (Grand & Helmberger 1984a) and the North Atlantic Ocean (Grand & Helmberger 1984b). The success of this SS waveform modeling in revealing the shear wave structure of the upper mantle beneath North America led LeFevre & Helmberger (1989) to include PP phases at upper mantle distances with direct P and crustal  $P_{nl}$  phases in developing an upper mantle P wave model (S25) appropriate for the Canadian Shield. WKBJ and Cagniard-de Hoop synthetics for P and  $P_{nl}$  waves for model S25 fit the observations very

satisfactorily. However, simplified WKBJ synthetics, involving only 'primary' ray sets like those used to model the direct P phases, do not match many of the PP data nearly as well. This appears to result from incomplete synthesis of the PP arrival rather than inadequacy of model S25. The contrasting success of simple WKBJ modeling of transverse SS waveforms (Grand & Helmberger, 1984a) further indicates that the P-SV system for multiple surface reflections is more complicated to model.

In this paper we perform a detailed analysis of the PP phase at upper mantle distances ( $25^\circ$  to  $60^\circ$ ; twice the corresponding upper mantle distance range for direct P) to better understand its propagation and the requirements for accurate synthetic modeling of the phase. We then use this insight to evaluate the usefulness of PP modeling in determining upper mantle structure. We find that the previous difficulty in matching observed PP waveforms is largely due to inadequacies in the simplified WKBJ computations that were made. Complete reflectivity synthetic seismograms, or more extensive WKBJ synthetics, can adequately account for the complexity of upper mantle PP phases, and provide a significantly improved fit to the data that enables further recovery of earth structure information. We present a variety of synthetic examples to elucidate the characteristics of the PP phase and establish its potential utility for interrogation of upper mantle velocity structure. We conclude with preliminary modeling of PP phases traversing the upper mantle beneath North America in which we resolve lateral variations in upper mantle P wave velocities beneath the continent.

## 2 SYNTHETIC PP WAVEFORMS AT UPPER MANTLE DISTANCES

Grand & Helmberger (1984a) and Lefevre & Helmberger (1989) have demonstrated that multiple surface reflections (PP, SS, SSS etc.) that turn in the upper mantle transition zone can be used to greatly extend our coverage of upper mantle structure. The primary advantages of these phases are that the upper mantle triplications of PP and SS are at twice the distance ( $25^\circ$  to  $60^\circ$ ) and have twice the time separation between triplication branches compared to the associated triplications of the direct P and S phases (observed at distances of  $12.5^\circ$  to  $30^\circ$ ). As a result, these phases have been valuable in determining velocity models for regions like the Canadian shield and East Pacific Rise, where only sparse direct phase coverage at upper mantle distances is available. The primary focus of previous research has been on identifying the upper mantle triplication (and quintuplication) arrivals in the multiple surface reflections. Figure 1 shows typical vertical component long-period WWSSN and Canadian Seismic Network recordings of P and PP waveforms from the October 18, 1967 Arctic event. These data were modeled by LeFevre &



Helmberger (1989) in the derivation of their Canadian shield P wave model, S25. These waveforms are at distances where direct P waves have bottoming points in the lower mantle, and any information about the upper mantle structure along the path must be derived from the shallower turning energy associated with the PP phase.

LeFevre & Helmberger (1989) calculated synthetic seismograms for the 1967 Arctic event using the WKBJ technique (Chapman 1978). In Figure 1, we show very similar synthetics for model S25 calculated in the same manner. Inspection of the observed waveforms and the WKBJ synthetics reveals that although the PP-P differential travel times are generally matched by this model, the synthetic PP waveforms do not closely resemble the data. The triplication arrivals predicted by the WKBJ synthetics for model S25 arrive in a narrow time window at distances from  $40^\circ$  to  $45^\circ$  (see stations SFA and OTT in Figure 1) resulting in large amplitude, relatively simple PP waveforms. Although the data do exhibit fairly simple waveforms at these stations, the polarities of the largest amplitude arrivals are actually reversed relative to the synthetics, and one would be hard-pressed to reliably identify the triplication features. At larger distances, the EF branch (energy turning below 670 km) and the AB branch (energy turning above 400 km) of the upper mantle triplications separate. This separation is apparent in the data, however, there are later arrivals with comparable amplitude that are not predicted by the WKBJ synthetics (e.g., OGD and GEO). This degree of waveform mismatch between data and synthetics makes it difficult to identify the onset of the emergent PP phase and its triplicated arrivals. The quality of the WKBJ synthetic fit to the PP data alone would provide little confidence in the details of model S25; LeFevre & Helmberger (1989) relied primarily on direct P and  $P_{nl}$  observations in the derivation of their model, with the PP-P timing being used essentially (and successfully) as a consistency check.

Synthetic waveforms computed with the reflectivity method for model S25 differ dramatically from the simple WKBJ synthetics, as shown in Figure 1, and provide much better fits to the PP data. Although the waveform modeling requires further improvement, the polarity of the PP waveforms at SFA and OTT is now correctly predicted, and the large amplitude arrivals following the AB branch at OGD, GEO, FLO and OXF are also accounted for. The comparison at OTT is particularly striking. The same triplications are present in the two synthetics, but the reflectivity synthetic predicts so much additional energy arriving in the overall PP waveform that even identifying the triplication branches is very difficult. However, the fact that the reflectivity synthetic resembles the data quite closely holds out hope for using the PP waveforms to study upper mantle structure. The reflectivity synthetics also produce a coda for direct P which was not included in the WKBJ synthetics, and which does not match the data very well. While the reflectivity

procedure is restricted to laterally homogeneous layers, and the crustal structure may in fact vary along the path, it is not surprising that model S25 produces such strong P coda. Later small arrivals between P and PP in the reflectivity synthetics are produced by underside reflections from upper mantle discontinuities that will be discussed below.

Grand & Helmberger (1984a) compared WKBJ synthetics with more accurate Cagniard-de Hoop generalized ray calculations (Wiggins & Helmberger 1974) for transverse SS phases at upper mantle distances and did not find a comparable extent of waveform incompatibility. Of course, both methodologies are ray-based, and similar truncated ray expansions were used in each method. The observation that the synthetics reproduce much of the observed waveform character does suggest that truncated ray expansions are sufficient for the SS phase. The PP phase is more complicated than transverse SS at upper mantle distances due to multiple P-SV conversions from interfaces near the source, receiver, and PP mid-path bounce point. The WKBJ synthetics computed by LeFevre & Helmberger (1989) and our own shown in Figure 1 include only the primary P and triplicated PP waves turning in the mantle and their corresponding depth phases. Phases reflected and/or converted from the Moho or strong transition zones within the crust are not included in these WKBJ synthetics, thus the synthetics are a partial calculation of the complete layered Earth response. It is well-established that at distances beyond  $70^\circ$ , where the PP phase turns in the lower mantle, simplified primary ray expansions in conjunction with a Hilbert transform produce PP synthetics that match observed data very well (e.g., Lynnes & Ruff 1985), but this apparently is not true at upper mantle distances. We found the degree of waveform error in the truncated synthetic calculations to be surprising, and were thereby motivated to conduct this analysis.

Figure 2 isolates the primary structural features affecting the discrepancy between the primary ray and complete synthetics by comparing P and PP synthetics calculated with WKBJ and reflectivity for simplified earth models. We make this comparison using the reflectivity method rather than generalized rays so that we do not need to specify a rayset and are ensured of including all important reverberations. These synthetics, and all others discussed in this section unless otherwise stated, are vertical component seismograms computed for a vertical dip-slip source (strike= $0^\circ$ , dip= $90^\circ$ , rake= $90^\circ$ ) at a depth of 18 km and convolved with a long-period WWSSN instrument response. The attenuation model from PREM (Dziewonski & Anderson 1981) is used in the computation of the reflectivity synthetics, while attenuation is included in the WKBJ synthetics by convolution with an anelastic attenuation operator (Futterman 1962) having a  $t^*$  value of 1.0 s. The synthetics in Figure 2 were calculated using the four different velocity models indicated: a smooth positive velocity gradient with no seismic discontinuities and no crustal layer (grad no

crust), the same model with a low velocity crustal layer (grad), a model with increasing velocities with depth with two upper mantle seismic discontinuities and no crust (disc no crust), and the same model with a crust (disc). The correspondence between synthetics computed for models that do not contain a low velocity crustal layer (grad no crust and disc no crust) is excellent, demonstrating that triplication effects are well accounted for by the WKBJ method as expected. However, the synthetics computed for models with a crustal layer are quite different. The largest discrepancy between the synthetics shown in Figure 2 occurs in the later part of the P and PP waveforms, indicating that the extra energy in the complete synthetics arises largely from multiple bounces in the crust. The waveform discrepancies are more pronounced for the model with upper mantle discontinuities because the multiple reverberations also triplicate, producing strong interference patterns. At distances larger than  $45^\circ$  this crustal complexity is manifested sufficiently late in the waveforms that the early part of the PP phase is not distorted, but this is clearly not the case at  $42^\circ$ , where the interference almost reverses the first strong PP upswing. This can easily lead to confusion when picking arrivals in the data.

In addition to crustal reverberations that dominate the later part of the PP waveforms, the Moho will also produce PP arrivals that reflect from its underside rather than from the free surface ( $P_mP$ ) and arrive prior to PP. Figure 3 shows the influence of these arrivals on PP waveforms as a function of propagation distance. Synthetic seismograms are calculated with the negative gradient velocity model illustrated in Figure 4. Waveforms in the top three rows are WKBJ synthetics that include the following rays: direct P, pP, sP and PP precursors reflecting up to three times from the bottom side of the Moho ( $P_mP$ ,  $P_mP_mP$ ,  $P_mP_mP_mP$ ); direct P, pP, sP, PP, pPP and sPP (PP); and a combination of the previous 2 raysets ( $P_mP+PP$ ). The Moho reflected PP energy precedes the PP phase out to distances of about  $40^\circ$ , producing waveforms ( $P_mP+PP$ ) that begin earlier and differ significantly from synthetics computed with the PP phase alone (PP). Beyond  $40^\circ$ , the Moho reflected phases have reduced amplitude and arrive simultaneously with PP, changing its waveform less dramatically. The bottom row in Figure 3 shows reflectivity synthetics which inherently include all of the reverberations. Comparison between WKBJ and reflectivity synthetics in the distance range where Moho reflected phases contribute to the PP waveforms indicates that these arrivals are indeed important, and are partially responsible for the incompatibility between the synthetic seismograms. The arrival between P and PP visible in all WKBJ synthetics but absent from the reflectivity synthetics is the B branch of the P wave triplication. The overestimation of WKBJ synthetic amplitudes in the shadow of triplications results from inadequacies of

Fresnel diffraction theory at the slowness of grazing rays and is well-established (e.g., Chapman & Orcutt 1985).

### *2.1 Whispering Gallery Modes*

For a positive velocity gradient in the uppermost mantle beneath the crust, Menke & Richards (1980) showed that the Moho can act as an efficient 'whispering gallery' interface, causing energy to propagate along it. We follow the convention of identifying phases as 'whispering gallery' arrivals,  $P_mP(WG)$ , only if they 'hug' the boundary at which they have underside reflections. Phases turning deeper in the upper mantle and reflecting from the underside of the Moho are termed  $P_mP$  as discussed in the previous section. Figure 5 schematically illustrates these phases. The generation of significant  $P_mP(WG)$  requires that the impedance contrast across the Moho be large enough to reflect the energy turned in the positive gradient. Menke & Richards (1980) demonstrated that for Earth models satisfying this criteria, the family of Moho whispering gallery phases can have significant amplitude relative to the direct P wave. At upper mantle PP distances ( $25^\circ$ - $60^\circ$ ), Moho whispering gallery phases can arrive between 15 and 150 s after the direct P wave, ahead of and overlapping the PP phase, and thus  $P_mP(WG)$  may also contribute to the mismatch apparent in Figure 1 between WKBJ and reflectivity synthetics.

Menke & Richards (1980) found that the velocity gradient within the lid is the most important parameter affecting the properties of  $P_mP(WG)$ . Therefore at certain distances, where the early part of the PP phase consists of whispering gallery arrivals, thorough analysis of PP waveforms may provide constraints on lid velocity gradient. We investigate this by comparing reflectivity synthetics computed for velocity models having positive gradient, negative gradient and constant lid velocities (Figure 4). The gradients are approximated by many thin homogeneous layers in the reflectivity calculations.

Reflectivity synthetics for the models in Figure 4 are shown in Figures 6 (long-period) and 7 (broadband). For long-period waveforms out to a distance of  $34^\circ$ , strong, impulsive arrivals are apparent between P and PP for the positive lid gradient synthetics, with weaker energy arriving at the same time in the constant lid velocity synthetics, and little energy being present in the waveforms for the negative lid gradient model (Figure 6). The impulsive arrivals in this distance range for the positive lid gradient involve whispering gallery phases that turn in the upper 165 km of the mantle. The whispering gallery phases are not observed for the negative gradient velocity model since no energy turns in the top 165 km. Beyond  $34^\circ$ , energy bottoming in the deeper positive velocity gradient below 165 km (Figure 4) and reflected from the bottomside of the Moho becomes the dominant arrival preceding PP for all of the velocity models. This phase corresponds to  $P_mP$  in Figure 3.

and the long-period signals beyond  $34^\circ$  are not diagnostic of the differences in lid velocity gradient. At distances closer than  $25^\circ$ , the whispering gallery arrivals produced by the positive lid velocity gradient model are obscured by the relatively large secondary branches of the direct P wave upper mantle triplication arrivals and P coda. Therefore long-period waveforms in the distance range between  $26^\circ$  to  $34^\circ$  are most sensitive to the velocity gradient in the lid, but it should be noted that our models are rather extreme. The more subtle long-period waveform differences for smaller variations in lid gradient could easily be missed in real data where lower signal to noise ratios are expected.

Menke and Richards (1980) showed that whispering gallery phases tend to lose much of their low-frequency energy through tunneling in the lower velocity material underlying the lid, making  $P_mP(WG)$  more prominent at shorter periods. This effect is apparent in broadband synthetics for the same models described above (Figure 7). The broadband synthetics for the positive lid velocity gradient model have  $P_mP(WG)$  arrivals with about ten times larger amplitude than the energy arriving at the same time for the negative lid velocity gradient model and twice the amplitude of the energy in the constant lid velocity synthetics for distances out to  $34^\circ$ . At distances between  $35^\circ$  and  $38^\circ$  the negative lid velocity gradient synthetics have *larger* amplitudes in the early part of the PP waveforms than synthetics for the other velocity models (Figure 7). This energy turns in the positive velocity gradient above the 400 km discontinuity and reflects from the bottomside of the Moho ( $P_mP$ ). The energy that was not turned in the lid for the negative lid gradient model strengthens the arrivals in this distance range, providing another possible diagnostic of the lid structure (note that in these calculations all of the models have similar velocity gradients from 200 to 400 km depth; see Figure 4). Beyond  $38^\circ$ , little  $P_mP$  precursory energy persists and synthetics for all of the velocity models resemble one another.

These calculations suggest that in the distance range  $26^\circ$  to  $38^\circ$  the variation in broadband PP waveforms predicted for upper mantle models with significantly different lid gradients is certainly large enough to detect in real data, if homogeneous paths are traversed. The variation in lid gradients represented in Figure 4 is almost certainly larger than we expect in the Earth; however, this exercise illustrates that analysis of the complete PP phase can potentially differentiate between positive and negative upper mantle lid gradients. Determination of the lid gradient is of profound importance for the high frequency propagation of regional phases like  $P_n$  (e.g., Sereno & Given 1990), which are used for earthquake and nuclear explosion discrimination. At larger distances, from  $38^\circ$  to  $60^\circ$ , energy that arrives between P and PP is mainly caused by underside reflections from deeper discontinuities ( $P_dP$ ), including the 400 and 670 km discontinuities. Neele &

Snieder (1991) demonstrate that this late P coda is quite coherent across small arrays, and waveform modeling of the  $P_dP$  phases can be used to constrain the discontinuities at the base of the lid and in the transition zone.

## *2.2 Crustal Reverberations*

Although explicit inclusion of whispering gallery modes and other bottomside Moho reflections in the WKBJ synthetics improves comparison with reflectivity synthetics for the early part of the PP waveforms (Figure 3), the high amplitude later part of the reflectivity PP waveforms is not yet accounted for. To determine what phases contribute to the large PP coda in the reflectivity calculations (and actual data), we added additional rays to the WKBJ synthetics (Figure 8). The synthetics in Figure 8 were computed using a velocity model with a slight positive gradient in the upper 200 km of the mantle overlain by a 6.4km/s, 40 km thick crust. The synthetics in the top row of Figure 8 (WKBJ1) were computed with the WKBJ procedure including only primary direct P and PP phases and their associated depth phases, pP, sP, pPP, and sPP. In addition to this rayset, the WKBJ2 synthetics include rays turning in the upper 400 km of the mantle and bouncing once from the underside of the Moho (this includes the first whispering gallery mode which is small due to the weak velocity gradient in the lid) and all rays having an extra reflection or conversion from both the free-surface and the Moho. The bottomside Moho reflected energy contributes to the beginning of the PP waveform as discussed in the previous section.

Inclusion of first crustal multiples begins to build the large amplitudes observed in the later part of the reflectivity PP waveforms, bringing the WKBJ and reflectivity synthetics into better agreement (Figure 8). This is especially apparent at distances larger than  $40^\circ$  where the waveforms are relatively simple. The P waveforms remain unchanged since the P wave crustal multiples were not included in the WKBJ calculations so that we could focus on the later arrivals. The agreement between WKBJ and reflectivity synthetics clearly improves with the addition of rays that have only one extra bounce in the crust. Additional improvement is expected as more crustal reflections and conversions are added until all possible interactions in a layered Earth have been accounted for. But, unfortunately, the convergence is rather slow at distances less than  $36^\circ$ , and ray-based procedures like WKBJ and Cagniard-de Hoope are tedious to implement. Of course, the primary advantage of building up the large ray files is that the ray-based methods are more readily modified to account for lateral heterogeneity (e.g., Helmberger et al. 1985). Because of the difficulty of identifying and including all significant rays in the WKBJ synthetics, and because our primary interest here is to understand basic characteristics of

the PP phase, we use the reflectivity method to compute the remaining synthetic seismograms in this study.

The crust exerts a strong influence on PP waveforms both by reflecting energy from its underside and by generating peg-leg multiples. Figure 9 illustrates the effects of variations in crustal thickness on P and PP waveforms. The synthetics are computed using the constant lid velocity model of Figure 4, with a single crustal layer having a thickness of either 20 or 40 km. Both long-period (top 2 rows) and broadband (bottom 2 rows) synthetic seismograms are shown to emphasize the waveform differences resulting from variations in crustal thickness. The waveforms and relative timing of P and PP phases change significantly as the thickness of the crustal layer decreases from 40 to 20 km. The PP/P amplitude ratio is strongly influenced by absolute velocities of the shallow crust, which will of course vary substantially. The thinner crust results in reduced PP-P travel times, a very important feature which could easily be misattributed to variation in average lid velocity. The timing of the PP arrival can also be confused by the arrival of the underside Moho reflections that precede and interfere with the PP phase, the nature of which is sensitive to mantle velocity gradients rather than average velocity values. In addition, actual differences in the average upper mantle P wave velocity structure will also result in PP amplitude and travel time variations.

The emphasis here has been on the early crustal reverberations that overlap the PP arrival and produce its early coda. This is generally called PP coupled PL, and is fairly coherent energy given the degree to which layered models can match details of the waveform. The later PP coda is known to become increasingly incoherent, with strong scattering contributions (Neele & Snieder 1991). It is difficult to assess how much of an isolated waveform should be interpreted in terms of any average crustal structure, and one must be rather conservative. In the real earth, lateral variations in crustal structure between the source, PP bouncepoint, and receiver regions is responsible for a breakdown in the redundancy of crustal reverberations, which is manifested in a ringing coda. Hybrid reflectivity procedures or laterally varying WKB methods (e.g., Helmberger et al. 1985) can be used to try to quantify some of these effects, but it is likely that a scattering formalism (e.g., Neele & Snieder 1991) is the best choice when the coda is found to be very complex. Broadband array measurements are the most promising approach to quantifying the PP coda behavior.

The many factors affecting PP travel times and waveforms make it difficult to attribute amplitude and travel time effects to one particular depth range in the Earth without some *a priori* information. In many regions *a priori* information on crustal thickness is known from refraction profiling. In this case PP-P arrival times and PP waveforms can be

modeled using complete synthetics to ascertain the average lid velocity structure. If broadband data are available, constraints on lid gradients may also be obtained. Next we illustrate the effectiveness of using PP phases to determine upper mantle structure by modeling long-period P and PP waveforms traversing North America. Crustal thicknesses beneath North America are fairly well known and we constrain this portion of our models using values compiled by Mooney & Braile (1989).

### 3 PP OBSERVATIONS AND WAVEFORM MODELING

Many waveform modeling studies of the seismic velocity structure in the upper mantle assume that raypaths travel primarily through laterally homogeneous material. For long-period waves traversing isolated geographic regions, this assumption is probably reasonable and the one-dimensional Earth models obtained have provided satisfactory fits to observed waveforms (e.g., Burdick 1981; Grand & Helmberger 1984a; Walck 1984; Lyon-Caen 1986). We rely on this approximation to model P and PP waveforms propagating through similar tectonic provinces in order to determine lateral variations in the upper mantle P wave velocity structure beneath North America. The advantages of using multiple bounce PP waves in conjunction with direct P observations to determine upper mantle structure are the increase in distance range sampling the upper mantle and reduction in source area anomalies caused by local structure or event mislocation through the use of differential arrival times. Extension of the distance range sampling the upper mantle is essential for modeling upper mantle structure beneath shield regions that are often devoid of earthquake sources. The disadvantages of modeling PP data are the added complication of this phase as discussed in the previous section and the relatively long propagation path of PP, which increases the likelihood of traversing laterally heterogeneous material. We try to minimize the effects of lateral heterogeneity on PP propagation by choosing source-receiver paths that remain primarily within one tectonic province.

Our data consist of long-period WWSSN and CSN seismograms for paths traversing North America. Although we have shown in the previous section that long-period waveforms have little sensitivity to velocity gradients in the upper mantle, PP-P travel times and gross features of the PP waveforms do contain information about the average velocity structure of the upper mantle, especially given the independent constraints on the structure provided by direct P modeling. Figure 10 shows our source-receiver geometry and Table 1 lists the source parameters of the earthquakes analyzed. Locations, depths and focal mechanisms for all of the sources were taken from the literature references



noted in Table 1. Earthquake source time functions were approximated as trapezoids with rise times and source durations determined from the inversion of teleseismic P waves.

### *3.1 Upper Mantle P Wave Velocity Models*

The earthquakes we use are all located in the tectonically active regions of Alaska, Mexico, and Central America and are recorded at stations located in the stable shield, platform, or tectonically active regions of North America (Figure 10). From S wave studies of the upper mantle beneath North America (e.g., Grand & Helmberger 1984a; Grand 1987; Wickens & Buchbinder 1980) and previous work on P waves (e.g., Burdick & Helmberger 1977; Burdick 1981; Dey-Sarkar & Wiggins 1976; LeFevre & Helmberger 1989; Wiggins & Helmberger 1973; Walck 1984) we expect upper mantle P wave velocities beneath the western U.S. to be slower than beneath the Canadian shield; however, little is known about the transition from one province to the other. To investigate lateral variations in P wave velocities beneath North America, we construct a suite of upper mantle P wave models ranging between the shield model S25 (LeFevre & Helmberger 1989) and the Gulf of California model GCA (Walck 1984). We then compare observed P and PP waveforms to reflectivity synthetics computed for each of the models to determine which best fits the data. Since crustal thickness in most tectonically active regions is thinner than in stable shield regions (Mooney & Braille, 1989) we assign crustal thicknesses of 20 km and 40 km to our tectonic and shield models respectively; however, we allow crustal thickness to vary if indicated by independent information or if required by the data.

The suite of velocity models used in our synthetic calculations is shown in Figure 11. We have slightly modified velocities from the published models S25 and GCA such that all models have the same velocities below a depth of 380 km. The velocity model between 380 km and 700 km was modified from S25 to best fit data sampling all of the tectonic regions. Below 700 km velocities are those of PREM. The two end-member models have about a 6% variation in P wave velocity in the upper 200 km of the mantle, resulting in PP-P travel times that can vary by as much as 10 s. Figures 12 and 13 compare some of the data (top row) to synthetic P and PP waveforms computed using the reflectivity method for several of the velocity models of Figure 11. Examples of waveforms from paths traversing the Canadian shield are shown in Figure 12 while signals traversing the North American platform and tectonically active regions are shown in Figure 13. The synthetic that best fits the data is shown in the second row of each column, just below the data trace. The lower two rows contain synthetics for the velocity models most similar to the one that best fits the data. All traces in Figures 12 and 13 are aligned on the P

wave arrival. Seismograms from paths in close proximity to one another and traversing the same geographic province are generally well fit by the same velocity model, giving us some confidence in the stability of the waveform comparisons.

For the nine paths traversing the northernmost Canadian shield, the waveform data are best fit by the fastest model, the slightly modified version of S25 (top row of Figure 12). Although an average crustal thickness of 40 km is reasonable for the Canadian shield (Mooney & Braille 1989), the model producing the next fastest travel times is Shld (Figure 11) with a 20 km thick crust. Figure 12 shows synthetic seismograms for velocity model Shld, with both a 40 and 20 km thick crust. The PP-P differential travel time and PP/P amplitude ratio produced by the latter two models are larger than observed at the closer stations (FBC and OTT in Figure 12), giving a worse fit to the data than model S25. By a distance of 490, where energy turning in the lower mantle constitutes the first arrival, model Shld with a 20 km thick crust matches the PP-P travel time but provides an inferior fit to the observed waveform when compared with model S25. The waveform at this distance recorded at station STJ from event 5 contains a clear later arrival from the AB branch of the upper mantle triplication that is best reproduced by the model S25 synthetic.

The bottom portion of Figure 12 shows data and synthetics for three of the six paths traversing the southern portion of the Canadian shield. These data are best fit by synthetics constructed with model Shld which has slightly lower velocities than S25 in the upper 200 km of the mantle (Figure 11). Synthetics computed for the faster model S25 have PP waveforms that begin sooner than indicated by the data and synthetics produced with the slower model Teca begin too late and have too small PP/P amplitude ratios. The transition from upper mantle P wave model S25 to Shld appears to occur quite abruptly with the seismogram from event 5 recorded at OTT best fit by the faster model and the seismogram from this same event recorded at the nearby station WES best fit by the slower model. This is compatible with the strong north to south gradients implied for shear velocity structure by the travel time station anomalies of Wickens & Buchbinder (1980) and the tomographic shear wave model of Grand (1987).

Paths crossing the North American platform also traverse crust with an average thickness near 40 km. Data from three of the five paths sampling the platform are shown in Figure 13 (top row) together with synthetic waveforms indicating that model Teca gives the best match to the observed seismograms. Both the travel times and waveforms of the faster model Shld and slower model Tecb provide poorer fits to the data. Data and synthetics for three paths sampling the tectonic province are shown at the bottom of Figure 13. Although the slowest model, GCA appears to be appropriate for many paths traversing the tectonically active regions of the western U.S. and Canada (Figure 13), this province is

the most heterogeneous and provides the least satisfactory agreement between observations and synthetics. We have found that adjacent raypaths sometimes have waveforms that are best fit by different velocity models. Crustal thickness in western North America can vary between 20 and 50 km over fairly short distances (Mooney & Braille 1989), thus, variations in crustal thickness at the source, receiver, and PP bounce-point may account for some of the difficulty in matching observations with one-dimensional models. Strong variations in upper mantle velocity structure, that are not accounted for by these laterally homogeneous models must also contribute to the waveform mismatch. Even given the difficulty of finding an average upper mantle velocity model that fits all of the data sampling the tectonically active regions of North America, it is clear that some of the data do require a velocity model as slow as GCA (Figure 13). This is somewhat surprising considering that GCA was derived from data sampling the actively spreading oceanic ridge in the Gulf of California, the tectonic province where we expect to find the slowest upper mantle velocities. This is one more line of evidence for the extreme nature of the upper mantle velocity structure under the basin and range province.

Waveform modeling of P and PP phases traversing North America indicates that a spectrum of velocity structures exist beneath North America. The fastest velocities are located beneath the northern Canadian shield, becoming progressively slower beneath the southern shield, North American platform, and the tectonically active areas of the western U.S.. The Canadian shield and continental platform are spatially coherent; PP data sampling broad regions of these provinces are well modeled by a single one-dimensional velocity structure. Given the complexity and structural sensitivity of the phases contributing to the overall PP waveform discussed in this paper it is remarkable that homogeneous structures can account for so much of the wavefield information. On the other hand, waveforms sampling the tectonically active regions of the western U.S. are not very well matched using any single one-dimensional model, indicating a higher degree of lateral heterogeneity at shorter horizontal scale lengths.

Upper mantle P wave velocity models for North America determined by several investigators using different data and techniques have provided strong evidence for the existence of lateral variations in the P and S wave velocity structure beneath the continent. Our study, which utilizes uniform data and methodology to investigate upper mantle P wave velocities beneath several different tectonic regions, supports the idea that strong lateral velocity gradients exist in the upper mantle beneath North America. The average upper mantle velocities we obtain for the different provinces of North America agree well with previous published velocity profiles determined for the same regions. PP waveforms traversing the northern Canadian shield require P wave velocities in the upper mantle to be

as fast as those of model S25 (LeFevre & Helmberger 1989) while waveforms crossing the southern shield are better fit by a velocity model having slower upper mantle velocities, similar to the stable North American continental model S8 (Burdick 1981). No single velocity model can satisfy all of the data traversing the tectonically active regions of North America; however, upper mantle velocities as slow as GCA (Walck, 1984) are required along some paths. We encountered little difficulty matching P and PP observations sampling all of the geographic regions with velocity models constrained to be identical below a depth of 380 km, and most of our models vary only in the upper 250 km. More extensive path coverage is required to explore the abruptness of lateral gradients in the upper mantle. Although the long-period PP waveforms are unable to constrain the exact depth and magnitude of the upper mantle discontinuities, it appears that large variations in these parameters are not required by the data.

#### 4 CONCLUSIONS

A detailed study of the PP phase at upper mantle distances has revealed that underside reflections from the Moho and crustal reverberations contribute significantly to PP waveform complexity. The failure of approximate synthetic seismogram techniques, such as WKBJ with only primary rays, to include these arrivals results in inaccurate PP seismograms and has been responsible for unsatisfactory agreement between PP observations and synthetics. More complete waveform synthesis of PP signals provides both improved modeling of the data and potential for extracting additional constraints on mantle structure. In the presence of a positive velocity gradient beneath the Moho, whispering gallery phases will arrive prior to PP at distances less than about  $34^\circ$ , while negative lid gradients lead to enhanced underside Moho reflections at distances from  $34^\circ$  to  $38^\circ$ . The short-period or broadband amplitudes of these underside Moho reflections are sensitive to the lid velocity gradient, providing a valuable diagnostic of upper mantle lid structure. Determination of the velocity gradient in the lid and its lateral variations is critical for understanding the composition of the upper mantle, and lid gradients also exert a strong influence on the frequency characteristics of regional phases. PP-P differential travel times and gross PP/P amplitudes are mainly sensitive to a combination of crustal properties and average upper mantle velocity structure. Crustal reflections and conversions at the source, receiver and PP mid-path bounce point interfere to produce large amplitude PP coda that is sensitive to crustal thickness. Given constraints on the crustal thickness, the PP-P differential travel time can be used to resolve average upper mantle velocity structure.

Using long-period waves traversing various tectonic portions of North America, we have shown that if crustal thickness is known *a priori* the average lid velocity can be determined. We find that a range in average P wave velocity models are appropriate for the upper mantle beneath North America. The highest velocities are located beneath the northern Canadian shield, with velocities becoming progressively slower beneath the southern Canadian shield, the stable continental platform and the tectonically active regions. Data from both the shield and platform areas are well-modeled with one-dimensional velocity structures, indicating that broad tectonically stable regions of the upper mantle are fairly homogeneous. Data traversing the tectonically active areas of North America can not be as satisfactorily modeled with a single velocity structure, but the average mantle velocities are certainly lower than beneath the craton and platform. Active tectonic processes occurring in these regions appear to have resulted in small scale velocity heterogeneity.

#### Acknowledgments.

We thank George Zandt, Brian Kennet, and Don Helmberger for helpful discussions during the course of this research and Jiajun Zhang for comments on the manuscript. Cray computer time was provided courtesy of George Zandt at Lawrence Livermore National Laboratory. This research was partially supported by NSF Grant EAR 8451715 and by The Department of the Air Force monitored by the Phillips Laboratory under Contract F19628-90-K-0041. Facilities support was provided by the W. M. Keck Foundation. This is contribution number 147 of the Institute of Tectonics and the C. F. Richter Seismological Laboratory.

## REFERENCES

- Burdick, L.J., 1981. A comparison of the upper mantle structure beneath North America and Europe, *J. Geophys. Res.*, **86**, 5926-5936.
- Burdick, L. J. & Helmberger, D. V., 1978. The upper mantle P velocity structure of the western United States, *J. Geophys. Res.*, **83**, 1699-1712.
- Burdick, L. J. & Orcutt, J., 1979. A comparison of the generalized ray and reflectivity methods of waveform synthesis, *Geophys. J. R. astr. Soc.*, **58**, 261-278.
- Chapman, C.H., 1978. A new method for computing synthetic seismograms, *Geophys. J.R. astr. Soc.*, **54**, 481-518.
- Chapman, C. & Orcutt, J., 1985. The computation of body wave synthetic seismograms in laterally homogeneous media, *Rev. Geophys.*, **23**, 105-163.
- Dey-Sarker, S. K. & Wiggins, R. A., 1976. Upper mantle structure in western Canada, *J. Geophys. Res.*, **81**, 3619-3632.
- Dziewonski, A.M. & Anderson, D.L., 1981. Preliminary reference Earth model, *Phys. Earth Planet. Inter.*, **25**, 297-356.
- Fuchs, K. & Müller, G., 1971. Computation of synthetic seismograms with the reflectivity method and comparison with observations, *Geophys. J. R. astr. Soc.*, **23**, 417-433.
- Futterman, W.I., 1962. Dispersive body waves, *J. Geophys. Res.*, **67**, 5279-5291.
- Grand, S. 1987. Tomographic inversion for shear velocity beneath the North American plate, *J. Geophys. Res.*, **92**, 14,065-14,090.
- Grand S.P. & Helmberger, D.V., 1984a. Upper mantle shear structure of North America, *Geophys. J.R. astr. Soc.*, **76**, 399-438.
- Grand S.P. & Helmberger, D.V., 1984b. Upper mantle shear structure beneath the Northwest Atlantic Ocean, *J. Geophys. Res.*, **89**, 11,465-11,475.
- Helmberger, D. V., 1973. Numerical seismograms of long-period body waves from seventeen to forty degrees, *Bull. Seismol. Soc. Am.*, **63**, 633-646.
- Helmberger, D. V., 1983. Theory and application of synthetic seismograms, in H. Kanamori and E. Boschi, Eds., *Earthquakes: Observation, Theory and Interpretation*, pp. 174-222, Soc. Italiana di Fisica, Bologna, Italy.
- Helmberger, D. V., Engen, G. & Grand, S., 1985. Notes on wave propagation in laterally varying structure, *J. Geophys.*, **58**, 82-91.
- House, L.S. & Jacob, K.H., 1983. Earthquakes, plate subduction and stress reversals in the eastern Aleutian Arc, *J. Geophys. Res.*, **88**, 9347-9373.
- LeFevre, L.V. & Helmberger, D.V., 1989. Upper mantle P velocity structure of the Canadian Shield, *J. Geophys. Res.*, **94**, 17,749-17,765.

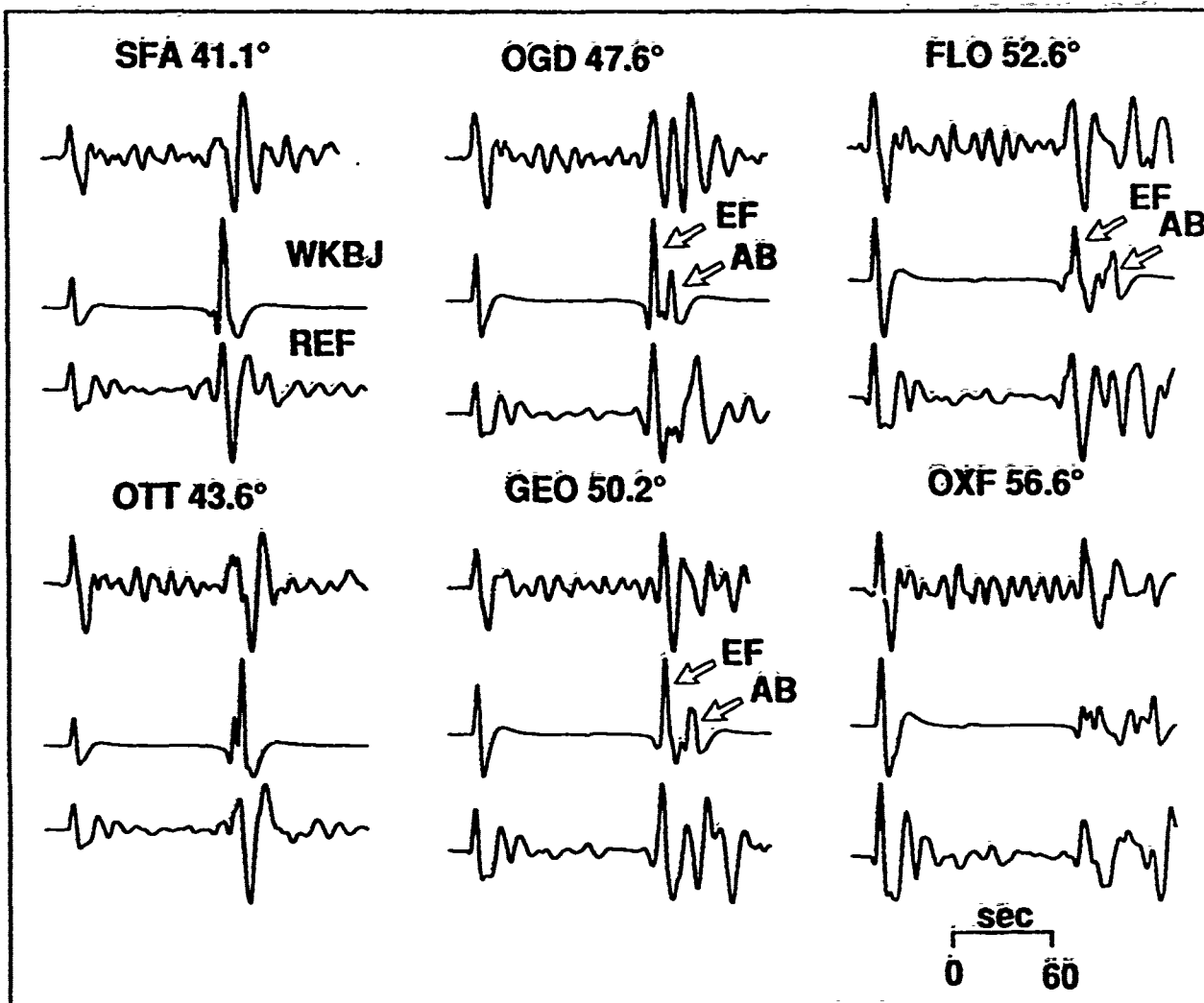
- Lynnes, C. S. & Ruff, L. J., 1985. Use of the PP phase to study the earthquake source, *Geophys. Res. Lett.*, **12**, 514-517.
- Lyon-Caen, H., 1986. Comparison of the upper mantle shear wave velocity structure of the Indian Shield and the Tibetan Plateau and tectonic implications, *Geophys. J.R. astr. Soc.*, **86**, 727-749.
- Menke, W.H. & Richards, P.G., 1980. Crust-mantle whispering gallery phases: A deterministic model of teleseismic  $P_n$  wave propagation, *J. Geophys. Res.*, **85**, 5416-5422.
- Mooney, W.D. & Braile, L.W., 1989. The seismic structure of the continental crust and upper mantle of North America, in Bally, A.W. and Palmer, A.R., eds., *The Geology of North America-An Overview*, vol. A, 39-52.
- Neele, F. & Snieder, R., 1991. Are long period body wave coda caused by lateral heterogeneity? *Geophys. J. Int.*, **107**, 131-153.
- Pennington, W.D., 1981. Subduction of the eastern Panama Basin and seismotectonics of northwestern South America, *J. Geophys. Res.*, **86**, 10753-10770.
- Perez, O.J. & Jacob, K.H., 1980. Tectonic model and seismic potential of the eastern Gulf of Alaska and Yakataga seismic gap, *J. Geophys. Res.*, **85**, 7132-7150.
- Richards, P. G., 1985. Seismic wave propagation effects-development of theory and numerical modeling, in A. U. Kerr, ed., *The Vela Program*, pp. 183-226, Executive Graphic Services, Washington, D.C..
- Sereno, T. J. & Given, J. W., 1990.  $P_n$  attenuation for a spherically symmetric earth model, *Geophys. Res. Lett.*, **17**, 1141-1144.
- Walck, M.C., 1984. The P-wave upper mantle structure beneath an active spreading center: The Gulf of California, *Geophys. J.R. astr. Soc.*, **76**, 697-723.
- Wickens, A. J. & Buchbinder, 1980. S-wave residuals in Canada, *Bull. Seismol. Soc. Am.*, **70**, 809-822.
- Wiggins, R. A. & Helmberger, D. V. 1973. Upper mantle structure of the western United States, *J. Geophys. Res.*, **78**, 1870-1880.
- Wiggins, R.A. & Helmberger, D.V., 1974. Synthetic seismogram computation by expansion in generalized rays, *Geophys. J. R. astr. Soc.*, **37**, 37-90.

Table 1. Earthquake Source Parameters

Event No.	Date	Lat (°N)	Long (°W)	Depth (km)	$m_b$	Strike (°)	Dip (°)	Rake (°)	$t_1$ $t_2$ $t_3$ (s)	Reference
1	5/17/64	59.40	142.70	10	5.1	329	15	135	1 1 1	PJ
2	7/1/67	54.44	157.94	12	6.1	94	72	5	1 2 2	HJ
3	6/15/68	5.64	82.60	5	6.0	3	82	180	.5 1 .5	P
4	8/18/70	60.70	145.38	15	5.8	348	15	164	2 2 2	PJ
5	7/3/73	57.99	138.04	13	6.1	295	24	84	2 2 2	PJ
6	4/7/83	8.0	82.69	15	5.5	311	22	113	1 1 1	HVD
7	5/9/83	8.28	82.93	7	5.5	332	31	142	2 3 2	HVD
9	10/13/84	15.06	94.24	16	6.1	290	22	70	.5 1 .5	HVD
10	12/20/84	11.44	86.16	15	5.4	296	21	84	1 6 1	HVD

locations from ISC, magnitudes from ISC (before 1983) or NEIC (after 1983), depths and source time histories ( $t_1, t_2, t_3$ ) from waveform modeling, focal mechanisms from P: Pennington, 1981; HJ: House and Jacob, 1983; PJ: Perez and Jacob, 1980; HVD: Harvard Centroid Moment Tensor.





**Figure 1.** Long-period P and PP observed seismograms (top trace), WKBJ synthetics (middle trace), and reflectivity synthetics (bottom trace) for the October 18, 1967 Arctic earthquake. The primary ray WKBJ synthetic PP waveforms computed for model S25 (LeFevre & Helmberger 1989) do not strongly resemble the data. Reflectivity synthetics for model S25 differ markedly from the WKBJ synthetics and more closely resemble the data. WWSSN and CSN station names and distances from the source are listed above each trace. AB and EF upper mantle triplication branches are marked where well separated.

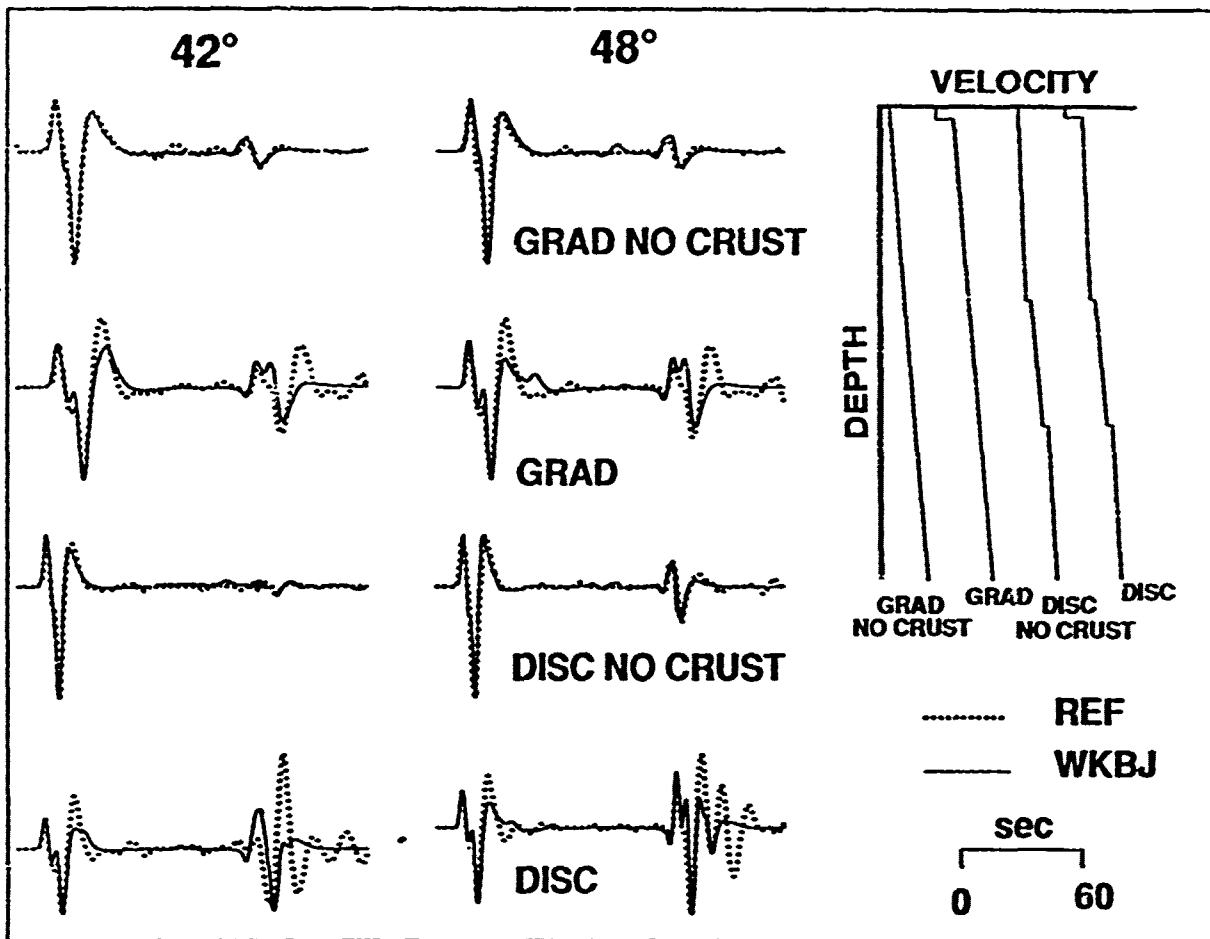


**Figure 2.** Comparison between reflectivity synthetics (dashed line) and primary ray WKBJ synthetics (solid line) for P and PP waveforms for a shallow (18km) vertical dip-slip source at distances of 42° and 48° for four upper mantle models schematically shown here. Note that the synthetics agree when no crust is included and the degree of mismatch is greatest for the model with both a crust and upper mantle discontinuities (disc).

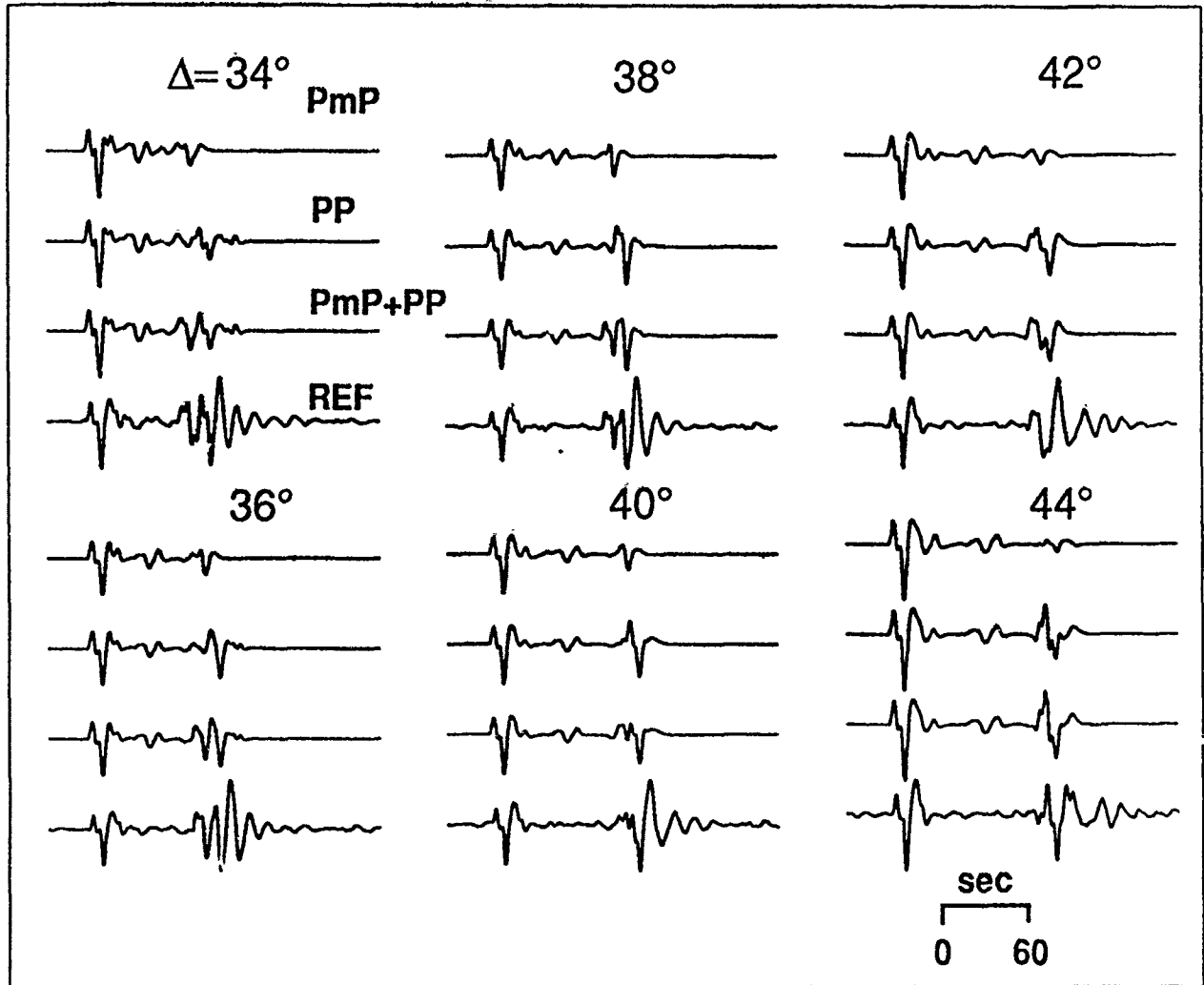


**Figure 3.** Synthetic seismograms computed for a shallow (18 km) vertical dip-slip source and the negative lid velocity gradient model of Figure 4 computed by: WKBJ including direct P, pP, sP and PP precursors reflecting up to three times from the bottom of the Moho ( $P_mP$ ); WKBJ with direct P, pP, sP, PP, pPP and sPP (PP); WKBJ with the combination of both raysets ( $P_mP+PP$ ); and reflectivity (REF). WKBJ synthetics computed with the more complete rayset ( $P_mP+PP$ ) more closely resemble the initial part of the reflectivity synthetics.

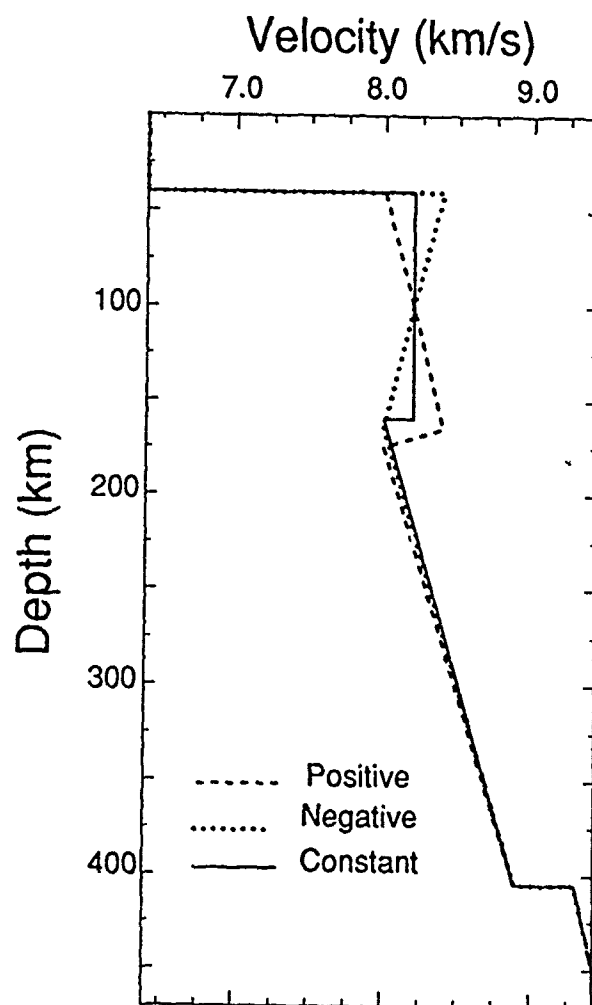


**Figure 4.** P wave velocity models with varying gradients in the lid just below the crust.

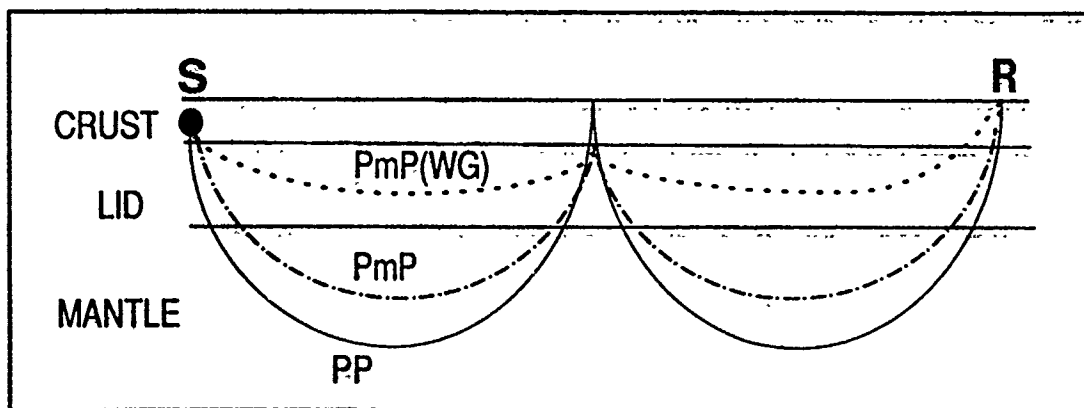


**Figure 5.** Schematic ray diagram of PP phase (PP), underside PP Moho reflection turning below the high velocity lid ( $P_mP$ ), and whispering gallery phase ( $P_mP(WG)$ ) hugging the Moho and turning in the positive velocity gradient in the lid.

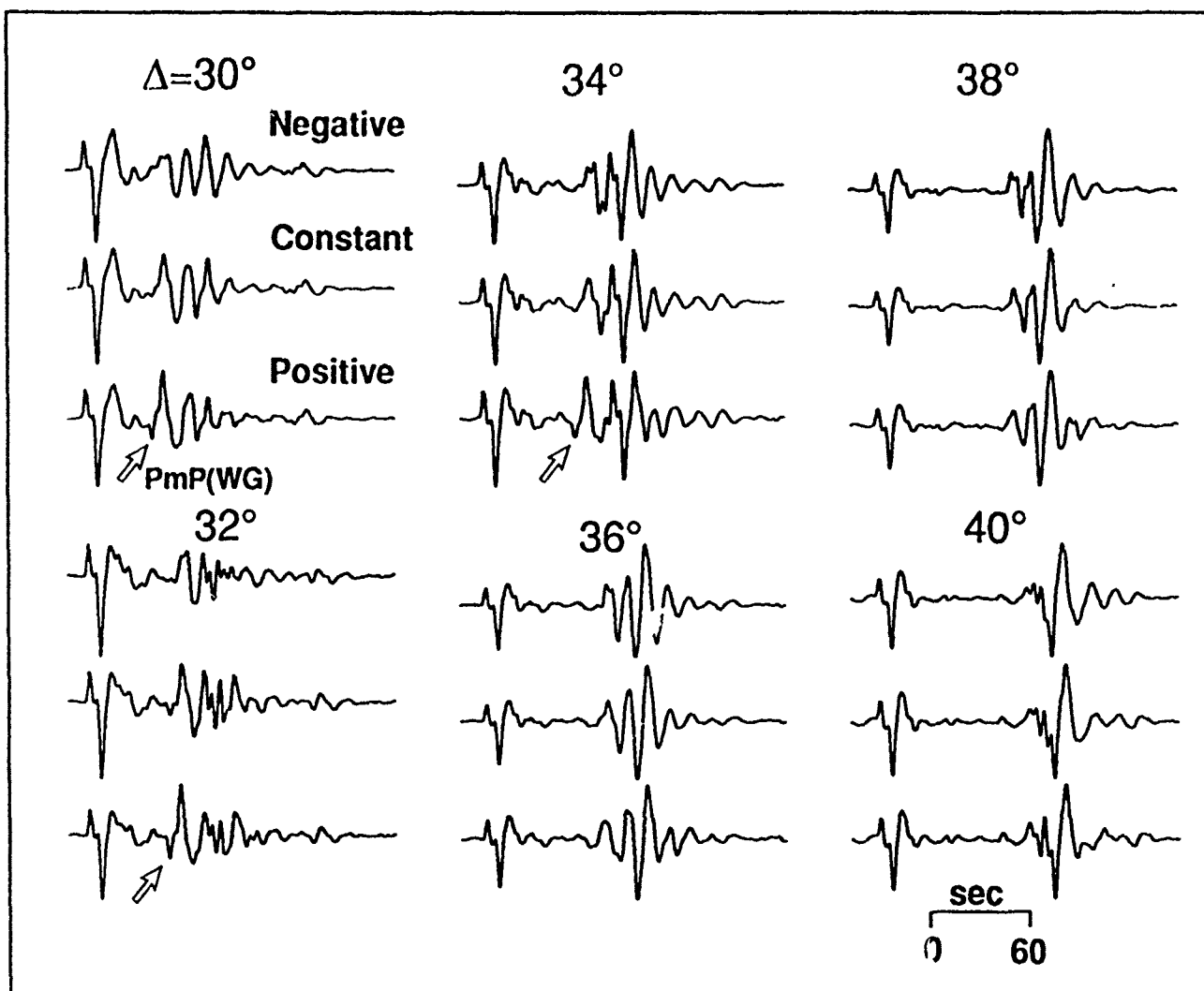


**Figure 6.** Long-period reflectivity synthetics computed for a shallow vertical dip slip source and the velocity models of Figure 4 having negative gradient, positive gradient, and constant lid velocities. Whispering gallery arrivals  $P_mP(WG)$  (indicated by the arrows) precede PP and are visible out to distances of about  $34^\circ$  in the synthetics computed for the positive lid gradient models.

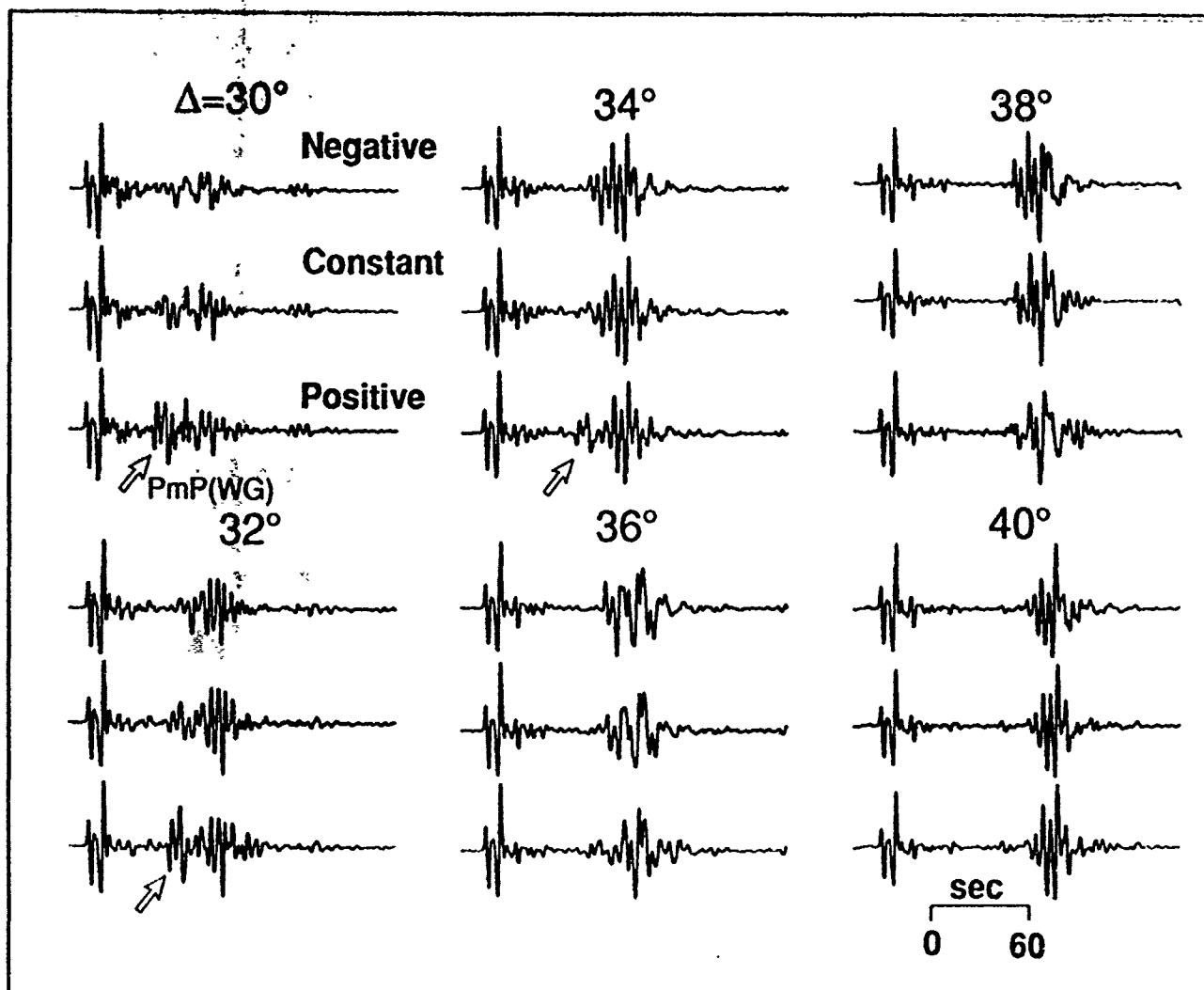


**Figure 7.** Reflectivity synthetics as in Figure 6 but convolved with a broadband instrument response. Whispering gallery phases  $P_mP(WG)$  (indicated with arrows) for the positive gradient velocity model are much more pronounced in the broadband seismograms.

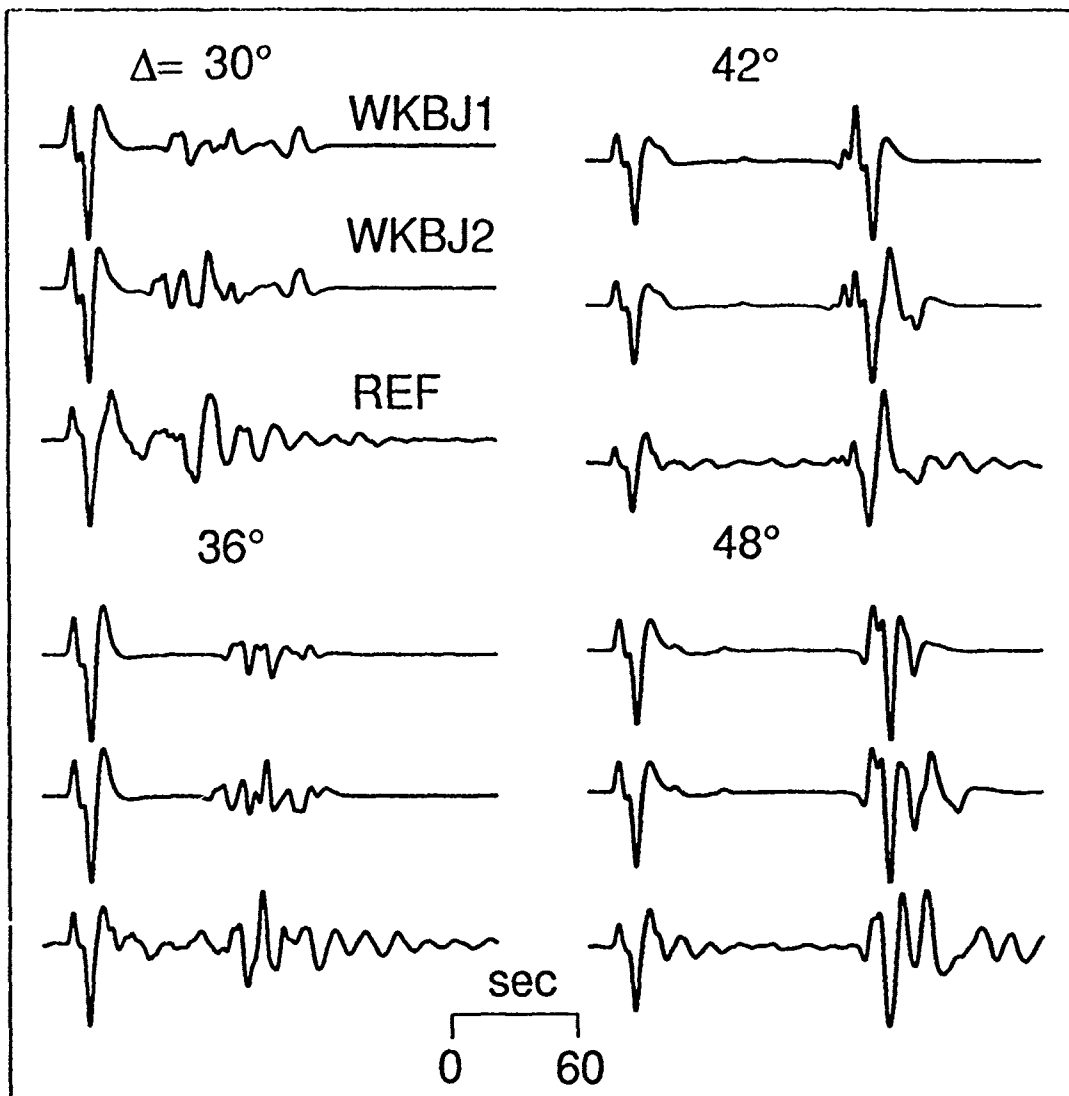


**Figure 8.** Synthetic seismograms computed for a shallow (18 km) vertical dip-slip source and a slight positive velocity gradient in the upper 200 km computed using: WKBJ including only direct P and PP rays and their associated depth phases (WKBJ1); WKBJ for the same rayset with additional rays turning in the upper 400 km of the mantle and bouncing once from the underside of the Moho (including the first whispering gallery mode) as well as all rays having an extra reflection or conversion from both the free surface and the Moho (WKBJ2); complete reflectivity (REF). Inclusion of the more complete rayset (WKBJ2) causes the WKBJ synthetics to more closely resemble reflectivity synthetics which include all reflections and conversions in a layered Earth.



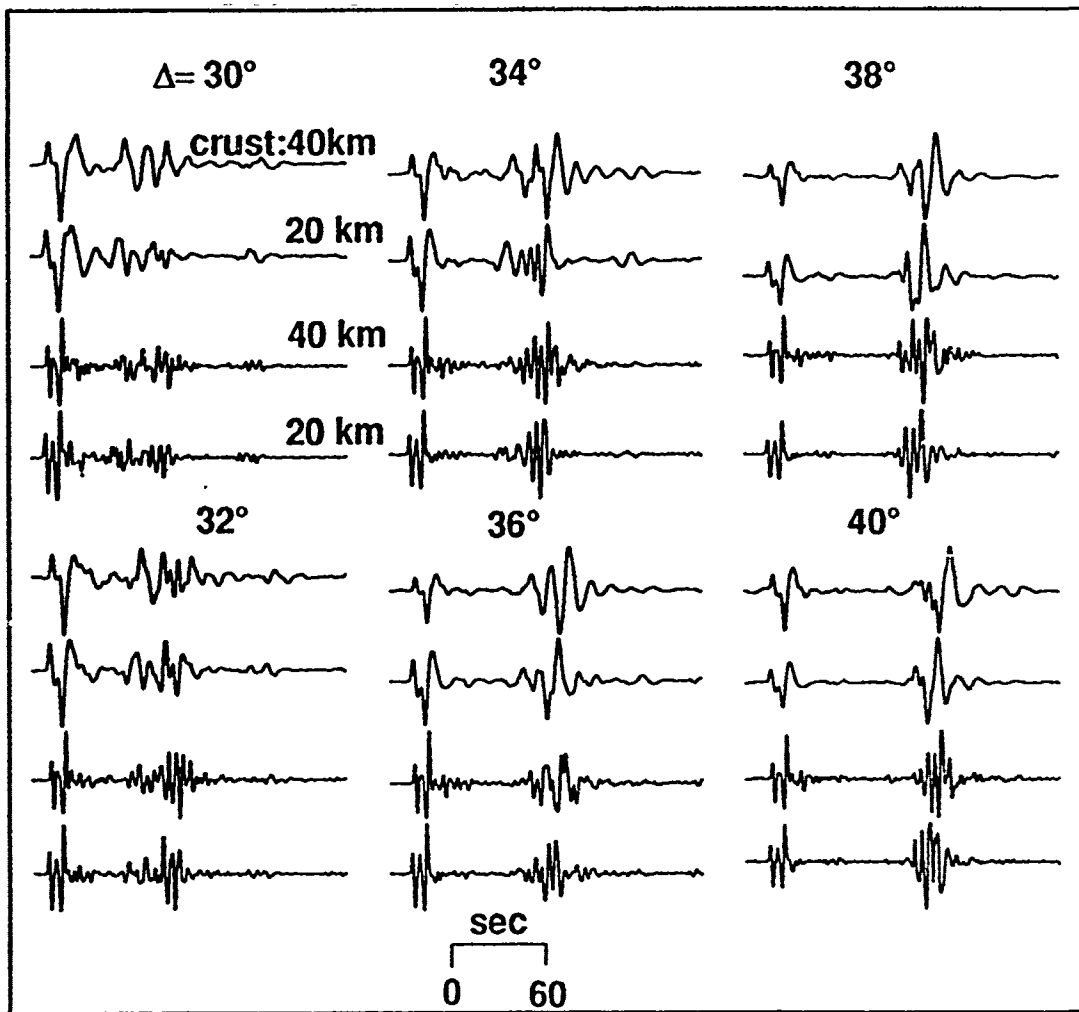


**Figure 9.** Long-period (top two traces) and broadband (lower two traces) reflectivity synthetics computed for a shallow vertical dip-slip source and the constant lid velocity model of Figure 4 underlying a single crustal layer with a thickness of either 20 or 40 km. Due to the large contribution of crustal multiples to the PP phase, changes in crustal thickness have a profound effect on PP waveforms. Waveform variations resulting from variations in crustal thickness are more clearly visible in the broadband synthetics.

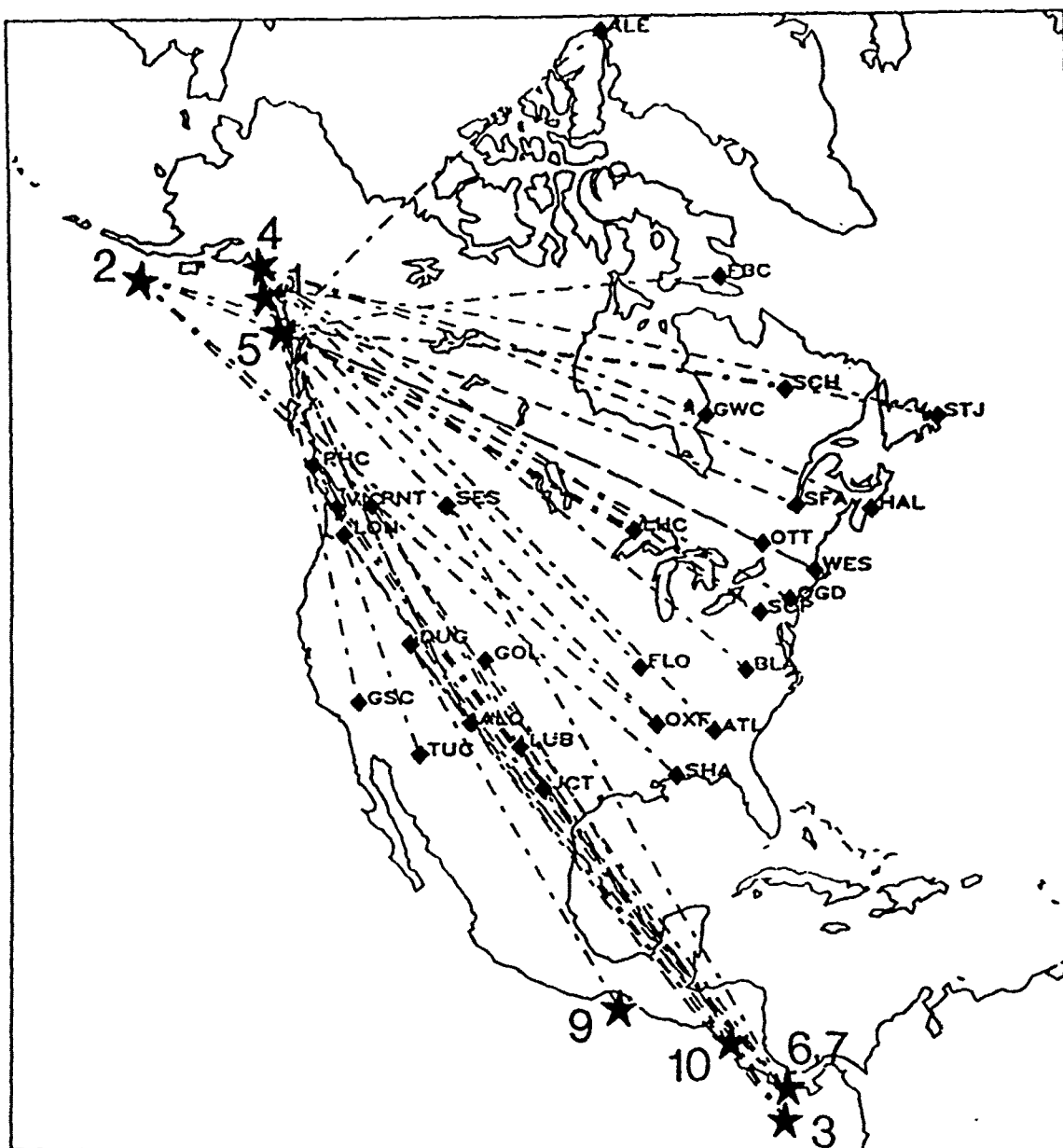


**Figure 10.** Location of earthquakes (stars) and North American stations used in this study.

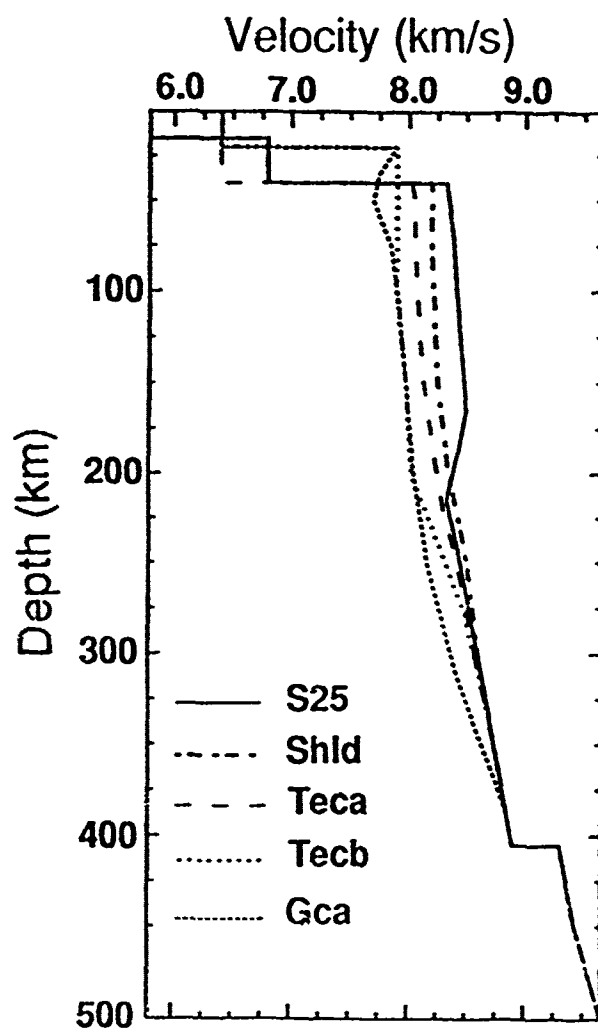


**Figure 11.** Suite of upper mantle P wave velocity profiles used to model data from North American paths.

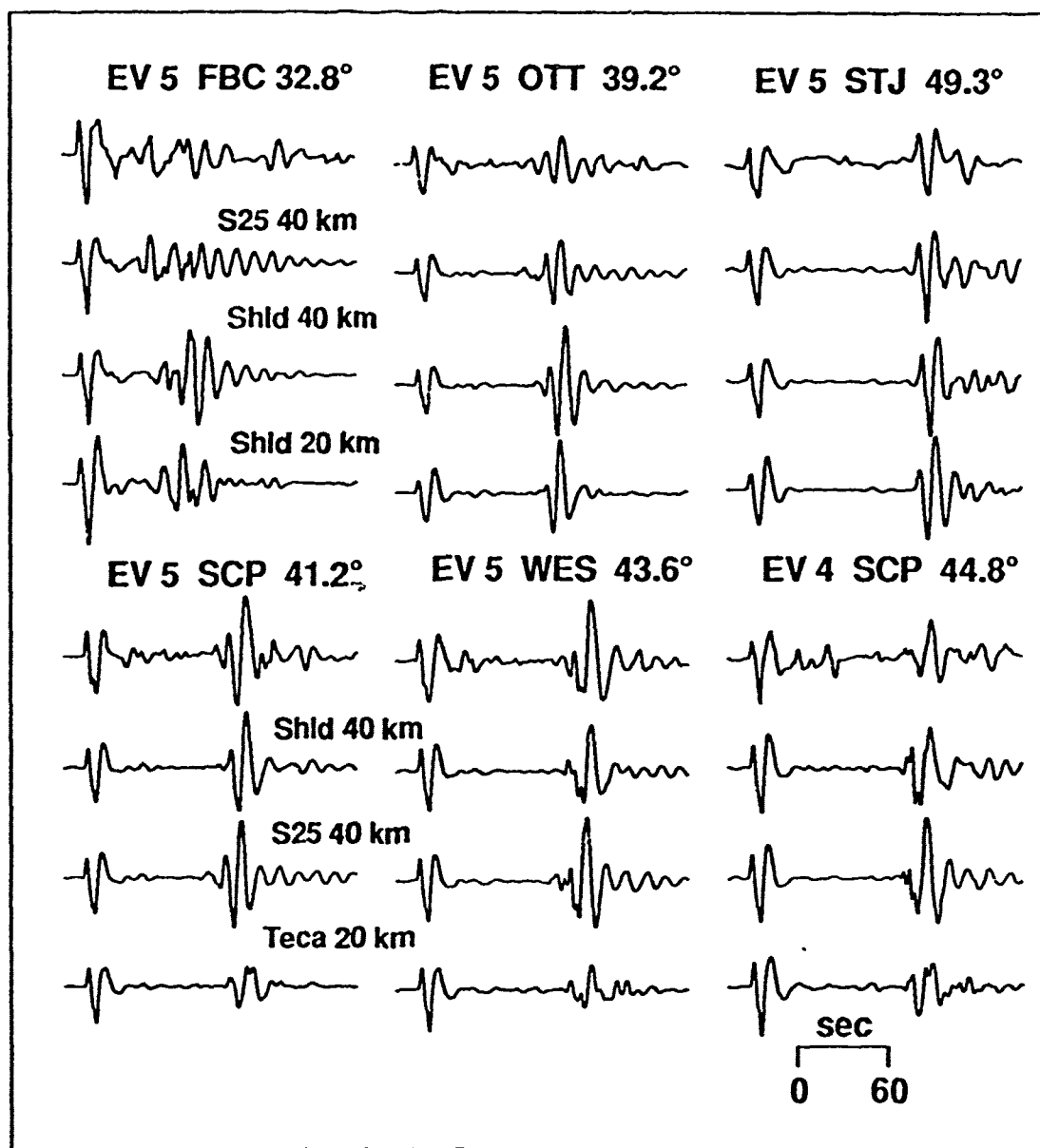


**Figure 12.** Observed and synthetic P and PP seismograms for paths traversing the northern (top panel) and southern (bottom panel) portions of the Canadian shield. The data are displayed in the top row of each column with the remaining rows indicating the synthetics that best match the data (second row) and those computed with the two velocity models most similar to the best fitting model (lower two rows). Waveform data sampling the northern portion of the Canadian Shield are best fit by the fastest model, S25, while data sampling the southern shield require a slower model, Shld.

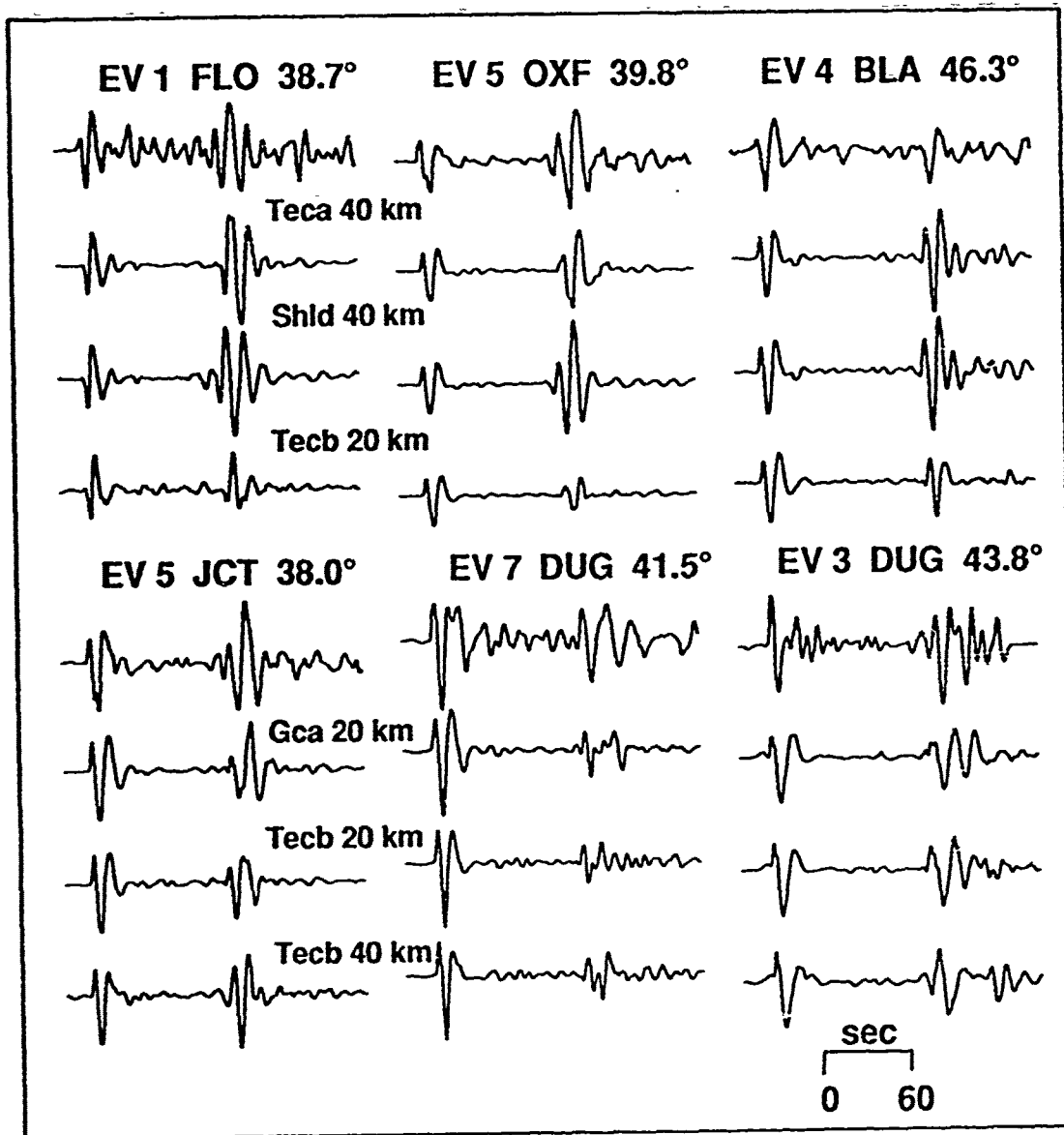


**Figure 13.** Similar comparisons to those in Figure 12 indicating that P and PP waveforms sampling the continental platform (top panel) require a velocity model slower than the southern shield region (Teca) and that data from the tectonically active areas of North America (bottom panel) sample upper mantle as slow as that found beneath the oceanic ridge in the Gulf of California (model Gca).

Prof. Thomas Ahrens  
Seismological Lab, 252-21  
Division of Geological & Planetary Sciences  
California Institute of Technology  
Pasadena, CA 91125

Prof. Keiiti Aki  
Center for Earth Sciences  
University of Southern California  
University Park  
Los Angeles, CA 90089-0741

Prof. Shelton Alexander  
Geosciences Department  
403 Deike Building  
The Pennsylvania State University  
University Park, PA 16802

Dr. Ralph Alewine, III  
DARPA/NMRO  
3701 North Fairfax Drive  
Arlington, VA 22203-1714

Prof. Charles B. Archambeau  
CIRES  
University of Colorado  
Boulder, CO 80309

Dr. Thomas C. Bache, Jr.  
Science Applications Int'l Corp.  
10260 Campus Point Drive  
San Diego, CA 92121 (2 copies)

Prof. Muawia Barazangi  
Institute for the Study of the Continent  
Cornell University  
Ithaca, NY 14853

Dr. Jeff Barker  
Department of Geological Sciences  
State University of New York  
at Binghamton  
Vestal, NY 13901

Dr. Douglas R. Baumgardt  
ENSCO, Inc  
5400 Port Royal Road  
Springfield, VA 22151-2388

Dr. Susan Beck  
Department of Geosciences  
Building #77  
University of Arizona  
Tucson, AZ 85721

Dr. T.J. Bennett  
S-CUBED  
A Division of Maxwell Laboratories  
11800 Sunrise Valley Drive, Suite 1212  
Reston, VA 22091

Dr. Robert Blandford  
AFTAC/TT, Center for Seismic Studies  
1300 North 17th Street  
Suite 1450  
Arlington, VA 22209-2308

Dr. G.A. Bollinger  
Department of Geological Sciences  
Virginia Polytechnical Institute  
21044 Derring Hall  
Blacksburg, VA 24061

Dr. Stephen Bratt  
Center for Seismic Studies  
1300 North 17th Street  
Suite 1450  
Arlington, VA 22209-2308

Dr. Lawrence Burdick  
Woodward-Clyde Consultants  
566 El Dorado Street  
Pasadena, CA 91109-3245

Dr. Robert Burridge  
Schlumberger-Doll Research Center  
Old Quarry Road  
Ridgefield, CT 06877

Dr. Jerry Carter  
Center for Seismic Studies  
1300 North 17th Street  
Suite 1450  
Arlington, VA 22209-2308

Dr. Eric Chael  
Division 9241  
Sandia Laboratory  
Albuquerque, NM 87185

Prof. Vernon F. Cormier  
Department of Geology & Geophysics  
U-45, Room 207  
University of Connecticut  
Storrs, CT 06268

Prof. Steven Day  
Department of Geological Sciences  
San Diego State University  
San Diego, CA 92182

Marvin Denny  
U.S. Department of Energy  
Office of Arms Control  
Washington, DC 20585

Dr. Cliff Frolich  
Institute of Geophysics  
8701 North Mopac  
Austin, TX 78759

Dr. Zoltan Der  
ENSCO, Inc.  
5400 Port Royal Road  
Springfield, VA 22151-2388

Dr. Holly Given  
IGPP, A-025  
Scripps Institute of Oceanography  
University of California, San Diego  
La Jolla, CA 92093

Prof. Adam Dziewonski  
Hoffman Laboratory, Harvard University  
Dept. of Earth Atmos. & Planetary Sciences  
20 Oxford Street  
Cambridge, MA 02138

Dr. Jeffrey W. Given  
SAIC  
10260 Campus Point Drive  
San Diego, CA 92121

Prof. John Ebel  
Department of Geology & Geophysics  
Boston College  
Chestnut Hill, MA 02167

Dr. Dale Glover  
Defense Intelligence Agency  
ATTN: ODT-1B  
Washington, DC 20301

Eric Fielding  
SNEE Hall  
INSTOC  
Cornell University  
Ithaca, NY 14853

Dr. Indra Gupta  
Teledyne Geotech  
314 Montgomery Street  
Alexandria, VA 22314

Dr. Mark D. Fisk  
Mission Research Corporation  
735 State Street  
P.O. Drawer 719  
Santa Barbara, CA 93102

Dan N. Hagedorn  
Pacific Northwest Laboratories  
Battelle Boulevard  
Richland, WA 99352

Prof Stanley Flatte  
Applied Sciences Building  
University of California, Santa Cruz  
Santa Cruz, CA 95064

Dr. James Hannon  
Lawrence Livermore National Laboratory  
P.O. Box 808  
L-205  
Livermore, CA 94550

Dr. John Foley  
NER-Geo Sciences  
1100 Crown Colony Drive  
Quincy, MA 02169

Dr. Roger Hansen  
HQ AFTAC/TTR  
Patrick AFB, FL 32925-6001

Prof. Donald Forsyth  
Department of Geological Sciences  
Brown University  
Providence, RI 02912

Prof. David G. Harkrider  
Seismological Laboratory  
Division of Geological & Planetary Sciences  
California Institute of Technology  
Pasadena, CA 91125

Dr. Art Frankel  
U.S. Geological Survey  
922 National Center  
Reston, VA 22092

Prof. Danny Harvey  
CIRES  
University of Colorado  
Boulder, CO 80309

Prof. Donald V. Helmberger  
Seismological Laboratory  
Division of Geological & Planetary Sciences  
California Institute of Technology  
Pasadena, CA 91125

Prof. Eugene Herrin  
Institute for the Study of Earth and Man  
Geophysical Laboratory  
Southern Methodist University  
Dallas, TX 75275

Prof. Robert B. Herrmann  
Department of Earth & Atmospheric Sciences  
St. Louis University  
St. Louis, MO 63156

Prof. Lane R. Johnson  
Seismographic Station  
University of California  
Berkeley, CA 94720

Prof. Thomas H. Jordan  
Department of Earth, Atmospheric &  
Planetary Sciences  
Massachusetts Institute of Technology  
Cambridge, MA 02139

Prof. Alan Kafka  
Department of Geology & Geophysics  
Boston College  
Chestnut Hill, MA 02167

Robert C. Kemerait  
ENSCO, Inc.  
445 Pineda Court  
Melbourne, FL 32940

Dr. Max Koontz  
U.S. Dept. of Energy/DP 5  
Forrestal Building  
1000 Independence Avenue  
Washington, DC 20585

Dr. Richard LaCoss  
MIT Lincoln Laboratory, M-200B  
P.O. Box 73  
Lexington, MA 02173-0073

Dr. Fred K. Lamb  
University of Illinois at Urbana-Champaign  
Department of Physics  
1110 West Green Street  
Urbana, IL 61801

Prof. Charles A. Langston  
Geosciences Department  
403 Deike Building  
The Pennsylvania State University  
University Park, PA 16802

Jim Lawson, Chief Geophysicist  
Oklahoma Geological Survey  
Oklahoma Geophysical Observatory  
P.O. Box 8  
Leonard, OK 74043-0008

Prof. Thorne Lay  
Institute of Tectonics  
Earth Science Board  
University of California, Santa Cruz  
Santa Cruz, CA 95064

Dr. William Leith  
U.S. Geological Survey  
Mail Stop 928  
Reston, VA 22092

Mr. James F. Lewkowicz  
Phillips Laboratory/GPEH  
Hanscom AFB, MA 01731-5000( 2 copies)

Mr. Alfred Lieberman  
ACDA/VI-OA State Department Building  
Room 5726  
320-21st Street, NW  
Washington, DC 20451

Prof. L. Timothy Long  
School of Geophysical Sciences  
Georgia Institute of Technology  
Atlanta, GA 30332

Dr. Randolph Martin, III  
New England Research, Inc.  
76 Olcott Drive  
White River Junction, VT 05001

Dr. Robert Masse  
Denver Federal Building  
Box 25046, Mail Stop 967  
Denver, CO 80225

Dr. Gary McCartor  
Department of Physics  
Southern Methodist University  
Dallas, TX 75275



Prof. Thomas V. McEvilly  
Seismographic Station  
University of California  
Berkeley, CA 94720

Dr. Art McGarr  
U.S. Geological Survey  
Mail Stop 977  
U.S. Geological Survey  
Menlo Park, CA 94025

Dr. Keith L. McLaughlin  
S-CUBED  
A Division of Maxwell Laboratory  
P.O. Box 1620  
La Jolla, CA 92038-1620

Stephen Miller & Dr. Alexander Florence  
SRI International  
333 Ravenswood Avenue  
Box AF 116  
Menlo Park, CA 94025-3493

Prof. Bernard Minster  
IGPP, A-025  
Scripps Institute of Oceanography  
University of California, San Diego  
La Jolla, CA 92093

Prof. Brian J. Mitchell  
Department of Earth & Atmospheric Sciences  
St. Louis University  
St. Louis, MO 63156

Mr. Jack Murphy  
S-CUBED  
A Division of Maxwell Laboratory  
11800 Sunrise Valley Drive, Suite 1212  
Reston, VA 22091 (2 Copies)

Dr. Keith K. Nakanishi  
Lawrence Livermore National Laboratory  
L-025  
P.O. Box 808  
Livermore, CA 94550

Dr. Carl Newton  
Los Alamos National Laboratory  
P.O. Box 1663  
Mail Stop C335, Group ESS-3  
Los Alamos, NM 87545

Dr. Bao Nguyen  
HQ AFTAC/TTR  
Patrick AFB, FL 32925-6001

Prof. John A. Orcutt  
IGPP, A-025  
Scripps Institute of Oceanography  
University of California, San Diego  
La Jolla, CA 92093

Prof. Jeffrey Park  
Kline Geology Laboratory  
P.O. Box 6666  
New Haven, CT 06511-8130

Dr. Howard Patton  
Lawrence Livermore National Laboratory  
L-025  
P.O. Box 808  
Livermore, CA 94550

Dr. Frank Pilotte  
HQ AFTAC/TT  
Patrick AFB, FL 32925-6001

Dr. Jay J. Pulli  
Radix Systems, Inc.  
2 Taft Court, Suite 203  
Rockville, MD 20850

Dr. Robert Reinke  
ATTN: FCTVTD  
Field Command  
Defense Nuclear Agency  
Kirtland AFB, NM 87115

Prof. Paul G. Richards  
Lamont-Doherty Geological Observatory  
of Columbia University  
Palisades, NY 10964

Mr. Wilmer Rivers  
Teledyne Geotech  
314 Montgomery Street  
Alexandria, VA 22314

Dr. George Rothe  
HQ AFTAC/TTR  
Patrick AFB, FL 32925-6001

Dr. Alan S. Ryall, Jr.  
DARPA/NMRO  
3701 North Fairfax Drive  
Arlington, VA 22209-1714

Dr. Richard Sailor  
TASC, Inc.  
55 Walkers Brook Drive  
Reading, MA 01867

Prof. Charles G. Sammis  
Center for Earth Sciences  
University of Southern California  
University Park  
Los Angeles, CA 90089-0741

Prof. Christopher H. Scholz  
Lamont-Doherty Geological Observatory  
of Columbia University  
Palisades, CA 10964

Dr. Susan Schwartz  
Institute of Tectonics  
1156 High Street  
Santa Cruz, CA 95064

Secretary of the Air Force  
(SAFRD)  
Washington, DC 20330

Office of the Secretary of Defense  
DDR&E  
Washington, DC 20330

Thomas J. Sereno, Jr.  
Science Application Int'l Corp.  
10260 Campus Point Drive  
San Diego, CA 92121

Dr. Michael Shore  
Defense Nuclear Agency/SPSS  
6801 Telegraph Road  
Alexandria, VA 22310

Dr. Matthew Sibol  
Virginia Tech  
Seismological Observatory  
4044 Derring Hall  
Blacksburg, VA 24061-0420

Prof. David G. Simpson  
IRIS, Inc.  
1616 North Fort Myer Drive  
Suite 1440  
Arlington, VA 22209

Donald L. Springer  
Lawrence Livermore National Laboratory  
L-025  
P.O. Box 808  
Livermore, CA 94550

Dr. Jeffrey Stevens  
S-CUBED  
A Division of Maxwell Laboratory  
P.O. Box 1620  
La Jolla, CA 92038-1620

Lt. Col. Jim Stobie  
ATTN: AFOSR/NL  
Bolling AFB  
Washington, DC 20332-6448

Prof. Brian Stump  
Institute for the Study of Earth & Man  
Geophysical Laboratory  
Southern Methodist University  
Dallas, TX 75275

Prof. Jeremiah Sullivan  
University of Illinois at Urbana-Champaign  
Department of Physics  
1110 West Green Street  
Urbana, IL 61801

Prof. L. Sykes  
Lamont-Doherty Geological Observatory  
of Columbia University  
Palisades, NY 10964

Dr. David Taylor  
ENSCO, Inc.  
445 Pineda Court  
Melbourne, FL 32940

Dr. Steven R. Taylor  
Los Alamos National Laboratory  
P.O. Box 1663  
Mail Stop C335  
Los Alamos, NM 87545

Prof. Clifford Thurber  
University of Wisconsin-Madison  
Department of Geology & Geophysics  
1215 West Dayton Street  
Madison, WS 53706

Prof. M. Nafi Toksoz  
Earth Resources Lab  
Massachusetts Institute of Technology  
42 Carleton Street  
Cambridge, MA 02142

Dr. Larry Turnbull  
CIA-OSWR/NED  
Washington, DC 20505

DARPA/RMO/SECURITY OFFICE  
3701 North Fairfax Drive  
Arlington, VA 22203-1714

Dr. Gregory van der Vink  
IRIS, Inc.  
1616 North Fort Myer Drive  
Suite 1440  
Arlington, VA 22209

HQ DNA  
ATTN: Technical Library  
Washington, DC 20305

Dr. Karl Veith  
EG&G  
5211 Auth Road  
Suite 240  
Suitland, MD 20746

Defense Intelligence Agency  
Directorate for Scientific & Technical Intelligence  
ATTN: DTIB  
Washington, DC 20340-6158

Prof. Terry C. Wallace  
Department of Geosciences  
Building #77  
University of Arizona  
Tuscon, AZ 85721

Defense Technical Information Center  
Cameron Station  
Alexandria, VA 22314 (2 Copies)

Dr. Thomas Weaver  
Los Alamos National Laboratory  
P.O. Box 1663  
Mail Stop C335  
Los Alamos, NM 87545

TACTEC  
Battelle Memorial Institute  
505 King Avenue  
Columbus, OH 43201 (Final Report)

Dr. William Wortman  
Mission Research Corporation  
8560 Cinderbed Road  
Suite 700  
Newington, VA 22122

Phillips Laboratory  
ATTN: XPG  
Hanscom AFB, MA 01731-5000

Prof. Francis T. Wu  
Department of Geological Sciences  
State University of New York  
at Binghamton  
Vestal, NY 13901

Phillips Laboratory  
ATTN: GPE  
Hanscom AFB, MA 01731-5000

AFTAC/CA  
(STINFO)  
Patrick AFB, FL 32925-6001

Phillips Laboratory  
ATTN: TSML  
Hanscom AFB, MA 01731-5000

DARPA/PM  
3701 North Fairfax Drive  
Arlington, VA 22203-1714

Phillips Laboratory  
ATTN: SUL  
Kirtland, NM 87117 (2 copies)

DARPA/RMO/RETRIEVAL  
3701 North Fairfax Drive  
Arlington, VA 22203-1714

Dr. Michel Bouchon  
I.R.I.G.M.-B.P. 68  
38402 St. Martin D'Heres  
Cedex, FRANCE

Dr. Michel Campillo  
Observatoire de Grenoble  
I.R.I.G.M.-B.P. 53  
38041 Grenoble, FRANCE

Dr. Jorg Schlittenhardt  
Federal Institute for Geosciences & Nat'l Res.  
Postfach 510153  
D-3000 Hannover 51, GERMANY

Dr. Kin Yip Chun  
Geophysics Division  
Physics Department  
University of Toronto  
Ontario, CANADA

Dr. Johannes Schweitzer  
Institute of Geophysics  
Ruhr University/Bochum  
P.O. Box 1102148  
4360 Bochum 1, GERMANY

Prof. Hans-Peter Harjes  
Institute for Geophysics  
Ruhr University/Bochum  
P.O. Box 102148  
4630 Bochum 1, GERMANY

Prof. Eystein Husebye  
NTNF/NORSAR  
P.O. Box 51  
N-2007 Kjeller, NORWAY

David Jepsen  
Acting Head, Nuclear Monitoring Section  
Bureau of Mineral Resources  
Geology and Geophysics  
G.P.O. Box 378, Canberra, AUSTRALIA

Ms. Eva Johannisson  
Senior Research Officer  
National Defense Research Inst.  
P.O. Box 27322  
S-102 54 Stockholm, SWEDEN

Dr. Peter Marshall  
Procurement Executive  
Ministry of Defense  
Blacknest, Brimpton  
Reading FG7-FRS, UNITED KINGDOM

Dr. Bernard Massinon, Dr. Pierre Mechler  
Societe Radiomana  
27 rue Claude Bernard  
75005 Paris, FRANCE (2 Copies)

Dr. Svein Mykkeltveit  
NTNF/NORSAR  
P.O. Box 51  
N-2007 Kjeller, NORWAY (3 Copies)

Prof. Keith Priestley  
University of Cambridge  
Bullard Labs, Dept. of Earth Sciences  
Madingley Rise, Madingley Road  
Cambridge CB3 0EZ, ENGLAND